Global Clinical Engineering Journal

Vol.6 Issue 3

Publisher International Medical Sciences Group, LLC

GlobalCE

open access

www.GlobalCE.org

ISSN: 2578-2762

GlobalCE

Editor's Corner

Building Better Healthcare: The Vital Role of Clinical Engineering in Hospital Construction

In the meticulous construction of a new hospital, every detail counts. From needs assessment and architectural design to the implementation of state-of-the-art medical technology, each element plays a crucial role in the hospital's functionality, efficiency, and ultimately, the quality of patient care delivered. Among these critical components are somewhat less appreciated (especially when functioned as expected) fixtures, fittings, and equipment (FFE), which require careful management to ensure seamless operation and optimal utilisation within the healthcare environment.

Below are some of the benefits accrued by ensuring that FFE is holistically considered from conception through to the operational phase of the new hospital.

Enhancing Patient Care and Safety:

Properly considered fixtures, fittings, and equipment contribute significantly to the delivery of high-quality patient care. Functional equipment and well-designed fixtures create a conducive environment for healthcare professionals to perform their duties efficiently, leading to better outcomes for patients.

Conducting comprehensive risk assessments throughout the hospital development process helps identify potential hazards, including ergonomic challenges, equipment issues such as connectivity, electrical hazards, and infection control vulnerabilities. Proactive mitigation measures such as ergonomic design principles, equipment safety protocols, and infection prevention strategies minimise the likelihood of accidents and adverse events. Knowledge of and adherence to regulatory requirements and industry standards, along with comprehensive staff training and education, ensures compliance and promotes a culture of safety awareness. Integrating safety principles and universal design concepts into the architectural layout and FFE selection enhances overall safety and accessibility, while continuous monitoring and improvement processes foster a culture of transparency and accountability. By addressing safety risks proactively, future-ready hospitals uphold the highest benchmarks of safety and quality, positioning themselves as trusted providers of healthcare services now and in the years to come.

Comprehensive Planning:

Comprehensive planning stands as the cornerstone of successful hospital construction endeavours, necessitating meticulous attention to detail from inception to fruition. During the initial stages, prioritising thorough planning and coordination ensures the seamless integration of fixtures, fittings, and equipment (FFE) into the building design. This entails engaging a diverse array of stakeholders, including architects, engineers, clinicians, facilities managers, medical device managers, and importantly, patients and the public, to assess FFE requirements comprehensively.

Operational Efficiency:

Efficient FFE selection entails considering factors like reliability, ease of maintenance, and compatibility with existing infrastructure, ensuring uninterrupted care delivery. Strategically placing equipment within the hospital environment optimises workflow patterns and minimises unnecessary steps, enhancing efficiency. For instance, proximity between diagnostic equipment and treatment areas streamlines processes and reduces patient wait times. Proactive maintenance schedules, including calibration and preventive repairs, sustain equipment functionality and mitigate unplanned downtime, optimising resource utilisation and operational efficiency.

Embedding technological advancements such as smart sensors and predictive analytics augments operational efficiency by enabling proactive decision-making, monitoring, and maintenance interventions. Leveraging real-time data insights facilitates early detection of inefficiencies

and potential equipment shortfalls, empowering healthcare facilities to optimise resource allocation and enhance patient care delivery. By integrating efficient FFE selection, strategic placement, proactive maintenance, and technological innovation, hospitals can cultivate environments that prioritise operational excellence and elevate the standard of patient care.

Anticipating Technological Advancements:

One of the key aspects of future readiness is anticipating technological advancements in medical equipment and healthcare delivery. By staying abreast of emerging technologies such as telemedicine platforms, artificial intelligence (AI) diagnostics, and robotic-assisted surgery systems, hospital planners can design infrastructure that accommodates these innovations. This may include incorporating flexible room layouts, modular equipment configurations, and advanced IT infrastructure to support interoperability, new diagnostic and treatment modalities, and data exchange.

Adapting to Changing Patient Demands:

As patient preferences and expectations evolve, hospitals must adapt their facilities to meet shifting demands for convenience, accessibility, and personalised care. Future-ready hospitals may incorporate amenities such as patient-controlled environments, decentralised care hubs, and integrated telehealth services to enhance the patient experience. Flexible FFE solutions that allow for rapid reconfiguration and scalability enable hospitals to respond dynamically to fluctuations in patient volumes and care delivery models.

Furthermore, by incorporating the patient and public voice into the planning process, hospitals gain invaluable insights into the practical needs and preferences of those who will ultimately utilise the facility. This collaborative approach fosters a sense of ownership and trust among stakeholders, ensuring that the hospital environment is designed with the end-users' perspectives in mind, ultimately enhancing patient satisfaction and overall experience.

embedding patient and public voices into the early stages of planning promotes needs identification, transparency and accountability, empowering communities to actively participate in shaping their healthcare infrastructure. By soliciting feedback on design elements, wayfinding systems, and accessibility features, hospitals can create environments that are inclusive and responsive to diverse needs. Moreover, involving patients and the public in decision-making processes fosters a sense of shared responsibility for healthcare outcomes, promoting community engagement and social cohesion. Ultimately this not only enhances the functionality and efficiency of hospital facilities but also strengthens trust, collaboration, and resilience within the healthcare system.

Sustainability and Resilience:

In light of environmental concerns and resource constraints, future-ready hospitals prioritise sustainability and resilience in their design and operations. Energy-efficient fixtures, renewable energy sources, and green building materials reduce carbon footprint and operational costs while promoting environmental stewardship. Additionally, resilient infrastructure designs, such as backup power systems and disaster preparedness measures, cybersecurity and data privacy, enhance the hospital's ability to withstand and recover from unforeseen events, ensuring continuity of care in times of crisis. Clinical engineering professionals should be engaged in addressing these concerns.

Collaboration and Innovation Ecosystems:

Future-ready hospitals embrace collaboration and innovation ecosystems that foster partnerships with industry stakeholders, research institutions, and technology providers. This further facilitates continuum of care that includes the home. By actively engaging with these networks, hospitals can access cutting-edge technologies, research findings, and best practices that inform decision-making and drive continuous improvement. This collaborative approach enables hospitals to remain at

the forefront of innovation and deliver state-of-the-art care to their patients.

In the dynamic landscape of healthcare delivery, the correct management of fixtures, fittings, and equipment is indispensable for ensuring the seamless operation of a new hospital build. By prioritising patient care, operational efficiency and safety, healthcare institutions can create an environment conducive to healing and innovation. Through meticulous planning, diligent execution, and ongoing maintenance, hospitals can uphold the highest standards of quality and excellence in healthcare delivery for the benefit of patients and healthcare professionals alike.

Indeed, the essence of a hospital transcends its architectural beauty; it lies in its ability to provide comprehensive healthcare services supported by the right equipment and infrastructure. A tent equipped with essential medical supplies, diagnostic tools, and skilled healthcare professionals can function as a makeshift hospital in times of crisis, delivering life-saving interventions where they are most needed. Conversely, a visually stunning building devoid of essential medical equipment serves merely as a hollow shell, unable to fulfil its purpose of healing and caring for the sick. Therefore, while architectural aesthetics are undeniably important, it is the integration of appropriate fixtures, fittings, and equipment that truly defines a hospital's capacity to deliver effective healthcare services and positively impact the lives of its patients.

Nata Zaman

Secretary General of Global Clinical Engineering Alliance and Equipping advisor for the New Hospital Programme, NHS England, UK

CONTENTS

Editor's Corner 2

Development of a Voice-Controlled Wheelchair for Physically Impaired Individuals 6

By Jenina R. Amoguis, Mabel A. Lingon, Edwin R. Arboleda, Airah Cahigan

Design a Mobile Application for the Maintenance of Hemodialysis Machines using Flutter Framework 18

By Badria Ibrahim Eisa, and Mohamed Yagoub Esmail

Comparative Performance of Low-Cost Portable Scanner in Pregnancy Profile Ultrasonography: A Promising Adjunct to Telemedicine 26

By Afroza Naznin, Muhammad Abdul Kadi, Fatima Begum, Khondkar Siddique-e Rabbani

Deep Learning and Photoacoustic Technology for Microcirculation Classification: Comparison Between Smoking and Nonsmoking Groups 37

Hui Ling Chua and Audrey Huong

Received December 18 2023, accepted May 6 2024, date of publication May 23, 2024

Development of a Voice-Controlled Wheelchair for Physically Impaired Individuals

By Jenina R. Amoguis, Mabel A. Lingon, Edwin R. Arboleda, Airah Cahigan

Department of Computer and Electronics Engineering, Cavite State University, Indang, Cavite, Philippines

ABSTRACT

Background and Objective: Traditional manual wheelchairs provide mobility to individuals with physical impairments but are poorly suited for individuals with a combination of physical and cognitive or perceptual impairments. Manual wheelchairs are more physically demanding than powered wheelchairs; however, powered wheelchairs require cognitive and physical skills that not all individuals possess. The general objective of this study is to develop a voice-controlled wheelchair that allows a disabled person to move around independently using a voice-recognition application that is interfaced with motors. The study will be beneficial for quadriplegic individuals who are paralyzed in both arms and both legs.

Material and Methods: This study aims to modify a standard wheelchair controlled by voice commands where the EasyVR 3 Voice Recognition Module, ultrasonic sensors, microcontroller, and 12V wiper motor were integrated. Based on the signal given by the motor driving circuit, the controller switches the motor accordingly. The added safety feature is the ultrasonic sensor that senses obstacles with a fall detection system and sends a signal to the microcontroller to stop the chair.

Results: Through testing and evaluation, the device's functionality was proven to meet the desired objectives, and the limitations of the device were concluded. The motors and sensors were also found to be 100% functional. The average speed of the wheelchair is 0.2 m/s, and it can move with the user weighing up to 80 kg. The wheelchair lifts at an angle of up to 10°. The overall acceptability of the unit, analyzed using statistical parameters like mean method and standard deviation analysis, gives a 4.53 average, 4.53 on usability, 4.07 on correctness, 4.37 on control, 4.50 on reliability, 4.33 on safety, and 4.8 on comfort, which means the unit meets the objectives.

Conclusion: Based on the evaluation results, the project met the given objectives. The system was able to move following the voice command given. The device also proved its functionality, responsiveness, usability, correctness, control, reliability, safety, and comfortability. While the current study demonstrates the feasibility of voice-controlled wheelchairs, future research should focus on improving the accuracy and robustness of voice recognition systems and the incorporation of sensory feedback mechanisms, such as haptic feedback or auditory cues.

Keywords – *Voice-controlled wheelchair, assistive technology, voice recognition, assistive devices, quadriplegia.*

INTRODUCTION

Wheelchairs have been a boon for people with physical impairments, but they may not be suitable for individuals with a combination of physical and cognitive or perceptual disabilities. While manual wheelchairs require more physical effort, powered wheelchairs require cognitive and physical skills that not everyone possesses.[1,2]

To address these challenges, researchers conducted a study and devised a solution. They created a device using readily available and affordable materials and developed a voice-controlled wheelchair for disabled individuals who cannot operate powered wheelchairs.

The general objective of this study was to develop a voice-controlled wheelchair for physically impaired individuals. Specifically, this study aimed to (a) design and construct the circuitry of the device; (b) modify a standard wheelchair; (c) integrate the Easy VR 3 shield, ultrasonic sensor, microcontroller, 12V wiper motor, and standard wheelchair for the device; (d) develop a program for the device; (e) test and evaluate the performance of the system through pilot testing; and (f) determine the cost of the developed system.

The wheelchair could be used by people who suffer from mobility disabilities, which include cerebral palsy, spinal cord injury, stroke, Parkinson's disease, arthritis, muscular dystrophy, multiple sclerosis, amputation, polio, or other conditions resulting in paralysis, muscle weakness, nerve damage, stiffness of the joints, strength and endurance, short stature, conditions like Osteogenesis Imperfecta ("brittle bones"), or lack of balance or coordination.[3–7] This device is also best for quadriplegic individuals who are paralyzed in both arms and both legs.[8]

The design project primarily focuses on recognizing a limited set of voice commands for direction control – five (5) in total - and two (2) voice commands for trigger and standby. It is not intended to perform any other tasks.

To evaluate the system's effectiveness, final testing was conducted involving 30 participants, including 25 individuals who underwent testing in a simulated environment and 5 people with mobility disabilities. The assessment measured the system's ability and responsiveness to execute commands accurately. The testing was carried out over two (2) weeks in Indang, Cavite, Philippines.

METHODS

This section outlines the important specifications of the materials utilized in the design project and the steps taken to create the voice-controlled wheelchair. Each material was carefully selected based on its functionality and compatibility with the other components.

The voice-controlled wheelchair comprises a standard wheelchair, DC motor, voice recognition module, sensors, motor driver, microcontroller, and battery. The standard wheelchair used is an alloy-type wheelchair that weighs only 13.1 kgs compared to a standard wheelchair that weighs up to 16 kgs. It is certified by Japan International Standards, with a JIS sticker labeled JIS T 9201:2006, specifying standards for manually propelled wheelchairs.

The motors used in the project were wiper motors. Compared to other DC motors, wiper motors are cheaper and provide high torque and low speed, making them ideal for wheelchair use. The voice recognition module that was used was an EasyVR version 3 shield. Anjum and Seetha[9] conducted a similar method where EasyVR version 3 shield was used as a voice-activated system for disabled people. Unlike voice recognition modules that only support speaker-dependent features, the EasyVR module supports speaker-dependent and speaker-independent features. Ultrasonic sensors were used because they are the only type of sensor that doesn't depend on lighting. These sensors use ultrasonic frequency to detect objects

The main component used in the motor driver was a PNP-NPN Darlington pair transistor. This fast-switching device can operate up to 10A, making it a better option than relays that cannot operate above 4Hz. The transistor can be easily controlled using pulse width modulation techniques. The microcontroller used in this project was a Gizduino V4.1. Arboleda et al.[10] used Gizduino AtMega644 for smart wheelchairs using touchpad and Android device. Compared to the Arduino Uno and Gizduino AtMega644, the Gizduino V4.1 is cheaper and more user-friendly, which was used in this design. Finally, the battery used was a 12V 17Ah lead acid battery. This battery is lightweight and cheap yet provides a high capacity.

Design of the Voice-Controlled Wheelchair

The microphone was placed slightly to one side of the mouth (Figure 1) and will then convert the voice signal to an electric signal. It was covered with a sponge to suppress echo and noise and compress the input voice.

FIGURE 1. The microphone is placed slightly to one side of the mouth.

The motor driver used was transistor-based. It has a high-current and voltage NPN and PNP Darlington pair. This provides faster switching capabilities compared to relays (8). It was connected to the back wheel and responded according to the given command of the microcontroller. Wiper motors were also used to provide mobility in the wheelchair. Using a chain, the wiper motors lead the direction of the back wheel, as shown in Figure 2. Through the use of a chain drive, the motor torque was increased. The wiper motor was not directly attached to the back wheel.

FIGURE 2. The chain used to connect the wiper and back wheel.

The sensors used were HC-SR04 ultrasonic sensors.[11] Compared to infrared and proximity sensors, this provides accurate readings on solid objects, even in dark or bright rooms. The sensors were placed on the front and rear of the wheelchair, and the wheelchair automatically stops when the sensor detects a drop in terrain ahead (e.g., stairs) or an obstacle. Specifically, two ultrasonic sensors were placed at the front: 1 facing the floor (to detect approaching stairs) and 1 below the wheelchair (to detect approaching obstacles in the lower left front area), both within 1–200 cm, as shown in Figure 3. Lastly, two were placed at the back: 1 facing the floor (to detect approaching stairs) and 1 below the wheelchair (to detect approaching obstacles in the lower back area) as shown in Figure 4.

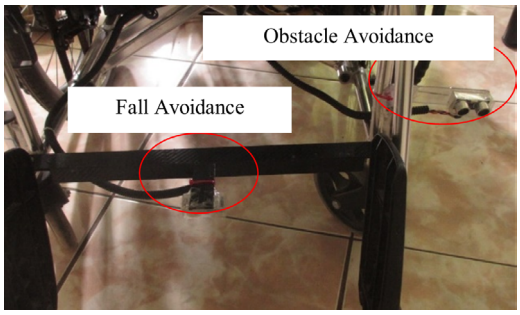

FIGURE 3. Attachment of front sensors.

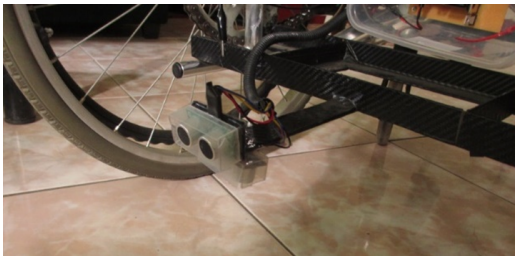

FIGURE 4. Attachment of back sensors.

Modifying a Standard Wheelchair

A standard wheelchair was used in the study. This provides a control unit, a battery, and a driver unit. These components were attached and transformed the wheelchair into a voice-controlled wheelchair. The control unit includes the microphone, rocker switch, and light-emitting diode (LED) indicator. The microphone was placed slightly on one side of the user's mouth. The LED indicators, shown in Figure 5, and the rocker switch were placed on the right armrest of the wheelchair. A fiberglass and sticker

were used to cover the LED indicator. The EasyVR 3, microcontroller, and battery were placed on the flat bar and plastic casing below the wheelchair. Figure 6 shows the flat bar attached to the wiper motors and battery. Flat bars were added on the lower front of the wheelchair where the sensors are attached. The plastic casing for the shields and motor driver was placed on the lower part of the wheelchair. The driver unit includes a motor driver circuit and 2 wiper motors. The wiper motor and the back wheel of the wheelchair were welded into a sprocket in a machine shop. A chain connected the sprockets found on the wipers and back wheels. This provides easier maneuvering of the wheelchair.

FIGURE 5. LED Indicators placed on the right armrest.

FIGURE 6. Flat bar attachment for wiper motors, battery, and ultrasonic sensor.

Integrating the EasyVR 3, Ultrasonic Sensor, Microcontroller, 12V Wiper Motor, and Standard Wheelchair for the Device

The user drives the wheelchair by giving voice commands converted to electric signals by the microphone and processed by the voice recognition module. The voice command is stored in memory and converted into digital signals using Analog-to-Digital Converters (ADC). The microcontroller receives the digital input, which then outputs a signal to the motor driving circuit, switching the motor accordingly. The ultrasonic sensor senses obstacle with a fall detection system and sends a signal to microcontroller to stop the chair. The block diagram of the voice-controlled wheelchair system is indicated in Figure 7.

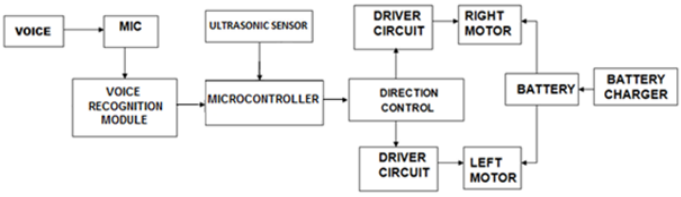

FIGURE 7. Voice-controlled wheelchair system block diagram.

The voice recognition module was soldered into a shield to provide an easy connection with the microcontroller. To connect the voice recognition module and microcontroller, the soldered voice recognition shield was attached to the Gizduino. A motor driver shield must be present since a motor cannot be directly connected to the microcontroller. This is an H-Bridge circuit that allows the microcontroller to control high-current motors. 4 input pins (2N222A transistor base in series with a 10KΩ resistor) were connected to the digital pins D5, D5, D9, and D10 of the microcontroller. The schematic of the motor driver and its physical connections are shown in Figures 8 and 9, respectively.

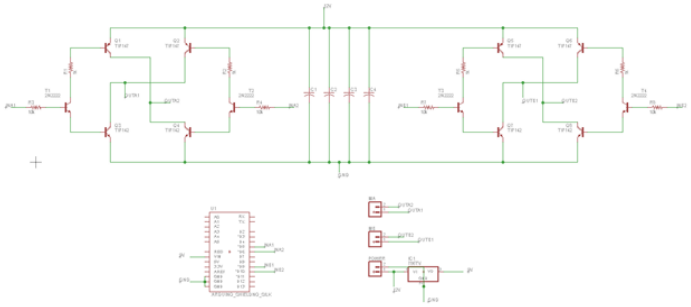

FIGURE 8. Motor driver schematic diagram.

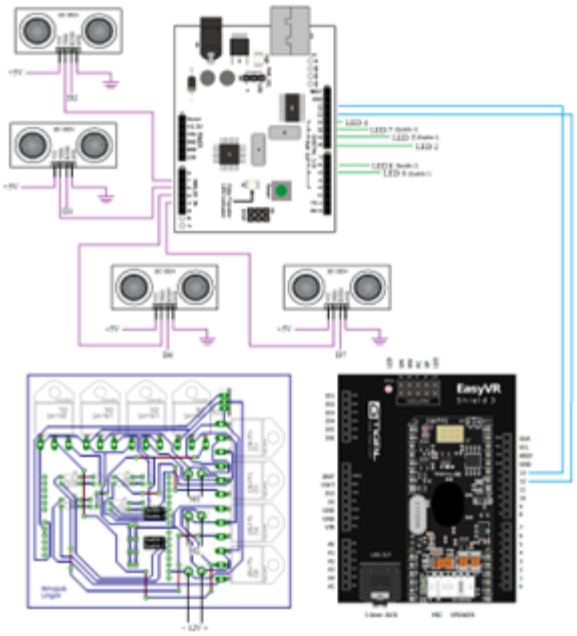

FIGURE 9. Physical connections of the device.

After connecting the EasyVR 3, ultrasonic sensors, microcontroller, and 12V wiper motor, the motors were attached to the flat bar between the front and back wheels. This was done in a machine shop. Lastly, the sensors, microcontroller, motor driver circuit, and voice recognition module were mounted below the wheelchair. A plastic casing was used in the final casing of the voice-controlled wheelchair circuitry. This way, the voice recognition module, ultrasonic sensors, microcontroller, motors, and wheelchair were integrated.

Developing the Program for the Voice-Controlled Wheelchair

The Arduino ATmega 328 microcontroller was programmed using C / C ++ language. This language was used to develop the software to control the wheelchair based on the data received from the voice recognition module. A predefined list of words controls the application with only a modest amount of RAM and program memory. The word list was created with the Arduino library. The Arduino is a PC-based program that lets users select and implement the user interface vocabulary. Those settings were recorded in memory. This memory was not lost even with the power off. The Voice Recognition Library provides an audio interface to a user's application program, allowing the user to control the application by uttering discrete words in a predefined word library. The words chosen for the library are relevant to the interaction between the application program and the user.

A word spoken through a microphone connected to the voice recognition module was analyzed on a frame-by-frame basis and quantized into feature vectors of sound characteristics against a vector codebook. The quantized feature vectors were then examined to determine which word they most closely match. The binary outputs were generated from the voice recognition module, which were set as a parameters for the program. The microcontroller received the converted voice from the voice recognition module. The application program takes appropriate action based on the parameters set by the developed program. However, once the obstacle and fall detection is active, the motors will automatically place the wheelchair in a safer place (Figures 10 and 11).

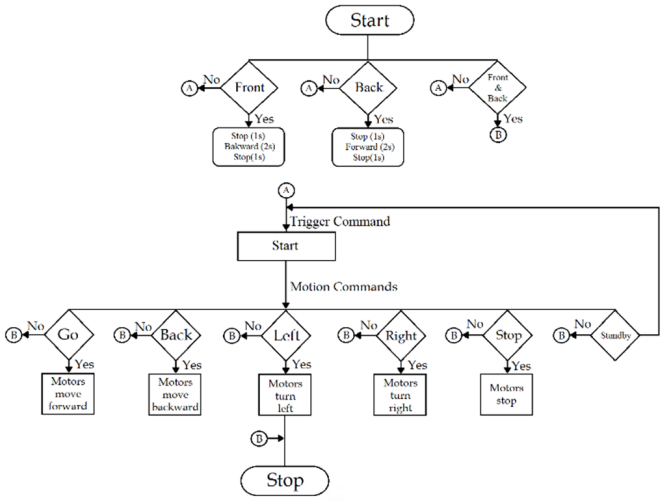

FIGURE 10. Software Flowchart for Speaker Dependent.

Project Testing

Before evaluating the wheelchair, the researchers pilot-tested the project. The project was tested in the Engineering Science Building, College of Engineering and Information Technology (CEIT), Cavite State University, Indang, Cavite, Philippines. The motors, voice recognition, and sensors were tested by giving different voice commands.

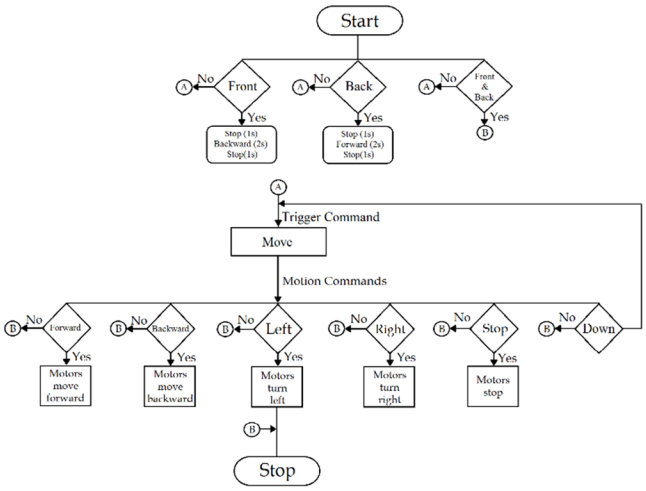

FIGURE 11. Software Flowchart for Speaker Independent.

Project Evaluation

The researchers evaluated the system's functionality in technical evaluation. This is done to identify if the operations that can be run on the wheelchair are attained. This includes tests for each sensor and motor integrated with the wheelchair. This way, the wheelchair is placed and tested in a quiet room with obstacles like chairs, walls, tables, and stairs. The second is placing the wheelchair in a room filled with random noise. All of these tests were repeated twice; the first is for speaker-independent, and the second is for speaker-dependent. The researchers identified which of these two features is more efficient.

In the acceptability test, the respondents conducted a final test on the device to evaluate usability, correctness, control, reliability, safety, and comfort by giving any desired voice command. This was done by gathering data from the respondents that used the device. The sampling method employed was opportunity sampling, whereby individuals from the target population who were available and willing to participate were selected to evaluate the device.[12] This includes a total of 30 respondents, which include 25 students selected from a sample of students at the CEIT and 5 persons who suffer from mobility disability. The respondents evaluated the device in a simulated environment. Each respondent was tied up in the simulated environment while using the device. To implement this, a hand and foot strap was provided on the wheelchair.

A clearance was sought first from the Ethics Review Board to ensure that the device was ready for Persons with Disabilities' (PWD) evaluation. They also gave any desired voice commands on the wheelchair.

The evaluation results are analyzed using statistical parameters like mean method and standard deviation analysis. Tables are used to present and discuss the results gathered.

Ethical Considerations

Prior to using the wheelchair, the researchers provided a detailed explanation of how it is operated. During the evaluation, no harm was done to any of the patients. A physical therapist also accompanied the researchers to provide medical assistance if needed. An informative document/manual was attached to the questionnaire to ensure the user was seated properly. The following parameters were taken into consideration: (a) The user is sitting upright in the chair; (b) The pelvic/seat belt is secured firmly; (c) The feet are placed flat on the ground; (d) The knees are aligned with the hips; (e) The trunk and pelvis are centered; (f) The head is centered with the chin slightly tucked; (g) The elbows are bent at a 90-degree angle; and (h) The chest is lifted.

Confidentiality and Informed Consent

Maintaining the participant's anonymity was also observed. They were not required to give their name or share personal information with the researchers. Moreover, the participants were given informed consent so that they could decide whether to participate or not.

PWDs' Evaluation Location and Compensation

Those participants who suffer from mobility disabilities were visited at General Emilio Aguinaldo Medical Hospital, Trece Martires, Cavite, Philippines. They were given compensation like a pack of assorted fruits. In answering the questionnaire, the patients were assisted by the researchers and his/her guardians.

RESULTS

Through this, the researchers could identify which voice recognition feature, speaker-dependent and speaker-independent, was more responsive. Moreover, as a possible strategy to reduce noise, the effect of wearing a helmet was also evaluated for both features.

The motors and sensors were found to be 100% functional. This was done by giving 10 trials per command and recording whether the voice was recognized successfully or not. The number of trials was based on the study titled "Design and Development of Voice Controllable Wheelchair," which also corresponds to the number of trial testing of the wheelchair's functionality.[13] The device's accuracy was proven good for speaker-dependent, while for speaker-independent, the accuracy was excellent. Table 1 shows the calculated rating for each word spoken through the EasyVR using the speaker-dependent feature. It has a low recognition rating for noisy environments, showing that the EasyVR is susceptible to noise.

TABLE 1. Functionality and Responsiveness Calculations Using Speaker-Dependent

	Noisy Environment	Quiet Environment
Spoken Word	No. of Correct Recognized Word	No. of Correct Recognized Word
Start	10	10
Go	4	10
Back	1	10
Left	1	10
Right	0	10
Stop	1	9
Standby	0	7
Average	24.29	94.29
Total Average	59.29	

Table 2 shows the calculated rating for each word spoken through the EasyVR using the speaker-independent feature. Comparing the results from Table 1, it can be shown that the EasyVR is less susceptible to noise using speaker independent.

TABLE 2. Functionality and Responsiveness Calculations Using Speaker-Independent

	Noisy Environment	Quiet Environment
Spoken Word	No. of Correct Recognized Word	No. of Correct Recognized Word
Start	9	10
Go	8	10
Back	6	10
Left	6	10
Right	5	10
Stop	7	10
Standby	7	10
Average	68.57	100
Total Average	84.29	

TABLE 3. Functionality and Responsiveness Calculations while Wearing a Helmet

Speaker Dependent		Speaker Independent	
Spoken Word	No. of Correct Recognized Word	Spoken Word	No. of Correct Recognized Word
Start	10	Move	10
Go	6	Forward	9
Back	1	Backward	6
Left	2	Left	7
Right	1	Right	7
Stop	3	Stop	8
Standby	1	Down	7
Average	34.29	Average	77.14

Table 3 shows the calculated rating for each word spoken through the EasyVR while wearing a helmet for both features. Comparing the results from Tables 1 and

2, it can be shown that the EasyVR is less susceptible to noise while wearing a helmet for speaker-dependent and speaker-independent.

Table 4 shows that the percent error of a well-trained speaker dependent is two times greater than the speaker-independent speech recognition. The error percentage was reduced by 10% when wearing a helmet for both features. The table suggests that the most effective feature is speaker-independent.

$$\text{Percent Error} = \frac{Words\ to\ be\ recognized - Words\ recognized}{Words\ to\ be\ recognized}\ x\ 100$$

TABLE 4. Comparison of Speaker Dependent and Speaker Independent

	Speaker Dependent	Speaker Independent
Software	The software learns the characteristics of the user's voice through training	It does not require training in the software
User	Works only to the trained user to recognize commands	Able to recognize commands by different users
Accuracy (% error)Noisy Environment	75.71%	31.43%
Accuracy (% error)Quiet Environment	5.71%	0 %
Reducing noise in wearing a helmet(% error)	65.71%	22.86%

The wheelchair's speed was calculated by dividing the distance travelled over time. It was determined that the wheelchair has an average speed of 0.2m/s with a person weighing 46 kilograms. The maximum weight capacity was determined by letting users with different weights, specifically, 46 kgs, 53 kgs, 61 kgs, 68 kgs, 72 kgs, and 80 kgs, sit on the wheelchair. With a user weighing 80 kgs, a noticeable decrease on the wheelchair's speed was observed. Figure 11 shows the effect of the user's weight on the wheelchair's speed.

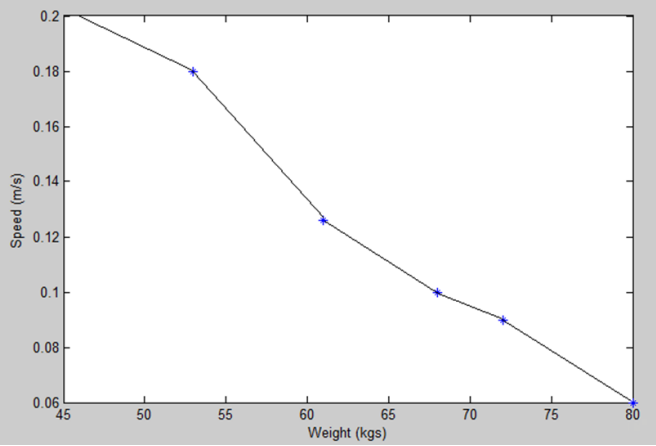

FIGURE 12. Speed versus weight.

The usability, correctness, control, reliability, safety, and comfort were gathered. A total of 30 respondents (25 students and 5 PWDs) were the participants who answered the questionnaire after they had used the wheelchair. Table 5 shows the user acceptability computations evaluated by 25 students at Cavite State University, Indang, Cavite, Philippines when the wheelchair was evaluated. It also shows that the usability, correctness, control, reliability, safety, and comfort of the wheelchair have low standard deviation. This means the device met the expected objective, and the system was considered efficient.

TABLE 5. User Acceptability Computations for Healthy Persons

General Qualities of the Wheelchair	Mean	Standard Deviation
Usability	4.6	0.58
Correctness	4.16	0.75
Control	4.4	0.71
Reliability	4.64	0.57
Safety	4.48	0.59
Comfort	4.84	0.47

Table 6 shows the user acceptability computations evaluated by 5 persons who suffered from mobility disability when the wheelchair was evaluated. PWDs evaluated it after the device was used by healthy persons and rated the device as acceptable. It also shows that the usability, correctness, control, reliability, safety, and comfort of the wheelchair have low standard deviation. This means that the device met the expected objective, and the system was considered efficient for persons with mobility disabilities.

TABLE 6. User Acceptability Computations for PWDs

General Qualities of the Wheelchair	Mean	Standard Deviation
Usability	4.2	0.45
Correctness	3.6	0.55
Control	4.2	0.45
Reliability	3.8	0.45
Safety	3.6	0.89
Comfort	4.6	0.55

Table 7 shows the overall user acceptability of the wheelchair. The mean and standard deviation evaluated by PWDs and students were combined.

TABLE 7. Overall User Acceptability Computations

General Qualities of the Wheelchair	Mean	Standard Deviation
Usability	4.53	0.57
Correctness	4.07	0.74
Control	4.37	0.69
Reliability	4.5	0.63
Safety	4.33	0.71
Comfort	4.8	0.48

Table 8 shows the actual cost of the voice-controlled wheelchair. This included the main parts of the device as well as the casing and screws. The unit cost was $369.48, comprising all materials essential to the device's construction.

TABLE 8. Total Cost of Device Construction

Materials	Quantity	Unit Cost (USD)	TOTAL COST (USD)
Microcontroller (gizDuino v3)	1	14	14
EasyVR Shield	1	52	52
Ultrasonic Sensor	4	5	20
12V 17Ah Lead Acid Rechargeable Battery	1	18	18
Battery Charger	1	15	15
Standard Wheelchair	1	79	79
TIP147	4	2	6
TIP142	4	1	4
2N222A	4	0.5	2
LM7809	1	0.4	0.4
Terminal Blocks	3	0.6	1.8
Resistor	8	0.035	0.28
12" × 12" Pre-sensitized Circuit Board	1	3	3
Wiper Motor	2	18	36
Chain	2	5	10
Sprocket	2	8	16
Plastic Casing	1	1	1
Labor	-	-	73
Miscellaneous Fees	-	-	18
TOTAL			$369.48

DISCUSSION

Wheelchairs are crucial for people with paralysis, muscle weakness, or any condition that limits their mobility. There are two types of wheelchairs: manual and powered. Manual wheelchairs require more physical effort, while powered wheelchairs demand cognitive and physical skills that not everyone possesses. To address this issue, researchers have developed a voice-controlled wheelchair that allows disabled individuals to move around independently. This wheelchair uses a voice recognition application connected to motors, enabling it to receive and perform voice commands given by the user. The microcontroller can be programmed to recognize a single user's voice or any voice command.

After conducting a technical evaluation, it was observed that the wheelchair was prone to noise, with only 17 out of 70 spoken words being recognized correctly as speaker-dependent and 48 out of 70 as speaker-independent. However, a helmet helped reduce noise and increased the number of correctly recognized spoken words to 24/70 for speaker-dependent and 54/70 for speaker-independent. This shows that wearing a helmet can significantly improve speech recognition accuracy. Furthermore, in situations with minimal noise, 66 out of 70 spoken words were recognized correctly for speaker-dependent and all 70 for speaker-independent. Hence, the speaker-independent feature was more accurate and responsive, and the survey was conducted using this feature.

The testing and evaluation of the wheelchair showed that it met the desired objectives and limitations of the device. The motors and sensors were fully functional, and the wheelchair could move at an average speed of 0.2 m/s, carrying a weight of up to 80 kg and lifting at an angle of up to 10°. The overall acceptability of the unit was rated at an average of 4.53, with ratings of 4.53 for usability, 4.07 for correctness, 4.37 for control, 4.50 for reliability, 4.33 for safety, and 4.8 for comfort. This indicates that the unit meets the objectives.

Due to its wiper motor design, the device only responds to stored voice commands and cannot be manually controlled. Ultrasonic sensors work well for detecting obstacles and stairs but have limited detection range and angle. The front sensor only detects obstacles on the left side, and the system cannot detect objects beyond 200 cm.

Table 8 presents the cost breakdown of the developed system, including the main components of the device as well as the casing and screws. The total unit cost was $369.48, covering all the necessary materials to construct the device.

Several studies and articled were synthesized to assess the effectiveness of the device. A research study, "Design and Development of Voice Controllable Wheelchair" published in 2022, is relevant to the methods and block diagram employed in this study for the voice-controlled wheelchair.[13] The study found that the Arduino analyzed the user's voice commands before transmitting the signal to the driver circuit which is similar to the process of this study, as depicted in Figure 7. Another study titled "Voice Controlled Automatic Wheelchair" produced similar positive outcomes to this research, although it used Arduino R3 as the wheelchair's primary processing unit.[14] A similar study titled "Development of a Low-cost Electronic Wheelchair with Obstacle Avoidance Feature" shows similar findings where ultrasonic sensors for obstacle avoidance and infrared sensors were also installed and thus gave out positive results concerning the individuals involved in the testing and evaluation.[15] The researcher compared the project's overall cost with a similar study called "Design of an Arduino Based Voice-Controlled Automated Wheelchair."[16] The cost of the mentioned study was close to the cost of the wheelchair developed in this study, indicating that the cost of components and materials used to develop this project is not too high. These studies validate the efficacy of the techniques and results in this research study, which contributes to the knowledge base of voice-automated wheelchairs.

Numerous studies have shown that access to independent mobility benefits children and adults. It enhances their educational and vocational opportunities, reduces their reliance on family members and caregivers, and promotes feelings of self-reliance.

CONCLUSIONS

Upon careful observation and analysis of gathered results, the Development of a Voice-Controlled Wheelchair for Physically Impaired Individuals has successfully met all desired objectives. The wheelchair is designed to respond to voice commands, allowing users to navigate and control the device through vocal instructions. With the capability to detect obstacles and stairs, the unit can automatically halt its movement, ensuring the safety and convenience of the user. This research study has demonstrated that technological advancements, particularly in trained and reprogrammed modules, can yield significant breakthroughs in the equipment used by patients in hospital wards. With proper orientation and guidance, individuals with physical impairments can operate a low-cost wheelchair using voice commands.

Recent advancements in technology have enabled patients to move independently without relying on the assistance of hospital staff or their loved ones. By utilizing voice commands, individuals with physical impairments can effortlessly control their movement, ensuring greater independence and convenience in their daily activities.

This research serves as a foundation for future studies, allowing for integrating more advanced technologies into voice-controlled wheelchairs. Ultimately, this study has the potential to improve the quality of life for individuals with physical impairments and those who aim to enhance the lives of individuals who cannot care for themselves effectively.

REFERENCES

1. Leaman Jand La HM. A Comprehensive Review of Smart Wheelchairs: Past, Present, and Future. IEEE Transactions on Human-Machine Systems, vol. 47, no. 4, pp. 486–499, Aug. 2017, doi: 10.1109/THMS.2017.2706727.
2. Kumar D, Malhotra R and Sharma SR. Design and Construction of a Smart Wheelchair. Procedia Computer Science 2020;172:302–307. doi: 10.1016/j.procs.2020.05.048.
3. Machol K et al. Hearing Loss In Individuals With Osteogenesis Imperfecta In North America: Results From A Multicenter Study. Am J Med Genet 2020;182(4):697–704. doi: 10.1002/ajmg.a.61464.
4. Sadowska M, Sarecka-Hujar B, and I. Kopyta. Cerebral Palsy: Current Opinions on Definition, Epidemiology, Risk Factors, Classification and Treatment Options. Neuropsychiatr Dis Treat 2020;16:1505–1518. doi: https://doi.org/10.2147/NDT.S235165.
5. Quadri SA, et al. Recent update on basic mechanisms of spinal cord injury. Neurosurg Rev 2020;(43)2:425–441. 2020, doi: 10.1007/s10143-018-1008-3.
6. Tan CEK, and Chao YX. Historical Perspective: Models of Parkinson's Disease. Internat J Molec Sci 2020;21:7. doi: 10.3390/ijms21072464.
7. Deguchi M, Tsuji S, Katsura D, et al. Current Overview of Osteogenesis Imperfecta. Medicina 2021;57(5). doi: 10.3390/medicina57050464.
8. Meyyazhagan A and Orlacchio A. Hereditary Spastic Paraplegia: An Update. Internat J Molec Sci 2022;23(3). doi: 10.3390/ijms23031697.
9. Anjum F and Seetha M. Voice-Activated System for Disabled People Using IoT. in Proceedings of the 2nd International Conference on Cognitive and Intelligent Computing, A. Kumar, G. Ghinea, and S. Merugu, Eds., Singapore: Springer Nature Singapore. 2023:219–226.
10. Arboleda ER, Paulite YVP and Carandang NJC. Smart Wheelchair with Dual Control using Touchpad and Android Mobile Device. Indonesian J Electric Engineer Informat 2018;6(1). doi: http://dx.doi.org/10.52549/ijeei.v6i1.342.
11. Elsokah M, Mejber AD, Zerek AR, et al. Next Generation of Smart Wheelchair with Speech Command. In The 7th International Conference on Engineering & MIS 2021, in ICEMIS'21. New York, NY, USA: Association for Computing Machinery, 2021. doi: 10.1145/3492547.3492758.
12. Berndt AE. Sampling Methods. J Hum Lact 2020;36(2):224–226. doi: 10.1177/0890334420906850.
13. Dutta PP, et al. Design and Development of Voice Controllable Wheelchair. In 2020 8th International Conference on Reliability, Infocom Technologies and Optimization (Trends and Future Directions) (ICRITO), Jun. 2020, pp. 1004–1008. doi: 10.1109/ICRITO48877.2020.9197765.

14. Umchid S, Limhaprasert P, Chumsoongnern S, et al. Voice Controlled Automatic Wheelchair. In 2018 11th Biomedical Engineering International Conference (BMEiCON), Nov. 2018, pp. 1–5. doi: 10.1109/BMEiCON.2018.8609955.

15. Bisognin A, et al. Ball Grid Array Module With Integrated Shaped Lens for 5G Backhaul/Fronthaul Communications in F-Band. IEEE Transactions on Antennas and Propagation vol. 65, no. 12, pp. 6380–6394, Dec. 2017, doi: 10.1109/TAP.2017.2755439.

16. Raiyan Z, Nawaz MS, Adnan AK, and Imam MH. Design of an arduino based voice-controlled automated wheelchair. In 2017 IEEE Region 10 Humanitarian Technology Conference (R10-HTC), Dec. 2017, pp. 267–270. doi: 10.1109/R10-HTC.2017.8288954.

Received January 10, 2024, accepted May 8 2024, date of publication May 31 2024.

Design a Mobile Application for the Maintenance of Hemodialysis Machines using Flutter Framework

By Badria Ibrahim Eisa, and Mohamed Yagoub Esmail

Sudan University of Science and Technologyi, Sudan

ABSTRACT

The hemodialysis machine is an artificial kidney facilitating the hemodialysis process and is considered a crucial life-sustaining device. Any delays resulting from malfunctions or improper maintenance of these machines can significantly impact the duration of dialysis for patients.

In Khartoum state, numerous highly skilled biomedical engineers are employed at dialysis centers, each with varying experience levels. However, the current training workshops provided to them are inadequate in ensuring proper maintenance of the machines. Many engineers struggle to address daily malfunctions and face challenges when referring to service manuals.

The recent proliferation of mobile applications has proven beneficial in several fields, particularly healthcare. This project will utilize a specific framework to develop a mobile application tailored to maintain hemodialysis machines. The app is designed to assist biomedical engineers in their daily tasks, particularly those in junior positions. By leveraging Flutter frameworks and the Dart language, a hybrid language capable of unifying code across Android, desktop, and iOS platforms, the "HDservice App" was created. This application offers detailed information on four common models of machine malfunctions in Sudan, along with corresponding solutions. Biomedical engineers have successfully integrated the app into their mobile devices, utilizing it for maintenance tasks. Subsequently, they conducted an evaluation comparing the app's effectiveness to that of traditional service manuals, yielding the desired outcome.

Keywords – *Hemodialysis machine, Maintenance, Mobile application, Flutter framework.*

INTRODUCTION

There are approximately 100 service engineers in Khartoum state, overseeing 1591 machines as reported in the latest inventory from the National Center of Kidney Diseases and Surgery in February 2023. This significant number of engineers managing a large quantity of machines, each with varying levels of experience ranging from 1 to 17 years, results in challenges related to supervision and training, particularly for junior engineers.

In the current landscape, mobile devices, such as smartphones and tablets, are prevalent among healthcare professionals, especially in light of the COVID-19 pandemic. Given the common occurrence of malfunctions in hemodialysis machines, there is an opportunity to consolidate maintenance procedures into a software package, such as a mobile app, to enhance the training program for engineers.

Hemodialysis Machine:

A dialysis machine works to filter a patient's blood. This process includes the removal of impurities and excess water.[1]

Hemodialysis machines have three basic functions:

1. Circulation of blood from the patient's access through the dialyzer and back to the access using a blood pump and a disposable tubing set.[2]
2. Preparation of dialysate from purified water and one or more concentrates and circulation of that dialysate through the dialyzer using a system that also controls the rate of fluid removal.[2]
3. Monitoring for any loss of integrity in either the blood or dialysate circuit or any excursion of an operating parameter outside a predefined range.[2]

Fault in Hemodialysis Machines:

Mechanical and electrical faults first cause faults in hemodialysis machines due to these five elements: pumps, power, transducers and sensors, pressure, and conductivity.[3]

And secondly, errors can arise from human error, such as misuse during operation or improper patient connection by nurses. These issues could be mitigated by ensuring that procedures are not initiated without full knowledge, particularly since they directly impact patient care. Biomedical engineers should also support nurses by offering comprehensive machine usage and maintenance training.

Furthermore, machine-related faults can also occur, underscoring the critical role of biomedical engineers in preventing risks associated with faulty or unchecked equipment. They must fulfill their responsibilities diligently and ensure that these machines remain operational for as long as possible during their duty cycles. As previously mentioned, their involvement in dialysis procedures and hemodialysis centers is crucial, with specific roles including:

1. Gain a comprehensive understanding of the operational mechanisms of hemodialysis equipment.[4]
2. Engage in the dialysis apparatus's operation, upkeep, repair, and sterilization.[5]
3. Take charge of ensuring the integrity of dialysis solutions, which involves overseeing electrolyte levels, osmotic pressure and conducting assessments for microbial/endotoxin presence.[5]
4. Participate in collaborative endeavors to enhance dialysis machinery and pioneer new treatment modalities with a proactive approach to disseminating findings through publications and conference presentations.[5]

Maintenance

Maintenance encompasses the activities undertaken to sustain equipment in its functional state, whether by averting its deterioration into a nonfunctional state or by restoring it to operation post-failure. This gives rise to a variety of maintenance practices that can be strategically planned to fulfill the maintenance goal, including preventive, predictive, or corrective measures.[6]

In hemodialysis facilities, to prolong the lifespan and efficiency of the machines, a focus on preventive maintenance is essential to reduce the frequency of corrective maintenance interventions.

Although disinfection procedures and decalcification are routinely conducted on weekends, the execution of corrective maintenance is lacking due to inadequate training programs, as highlighted in the identified issue.

Computerized Maintenance Management System (CMMS):

A CMMS is a sophisticated software solution that houses a comprehensive computer database containing vital information about an organization's maintenance operations. Within healthcare technology management, the CMMS serves as a tool for streamlining the documentation of all tasks associated with medical equipment, encompassing equipment scheduling, inventory supervision, corrective and preventative maintenance protocols, spare parts regulation, service agreements, and medical equipment notifications.[7]

Flutter Frameworks:

Reasons for Choosing Flutter Framework: Flutter is a cutting-edge application development framework developed by Google for building cross-platform mobile applications that can run on both iOS and Android operating systems. As detailed on the official website (https://flutter.io/), it was selected for its primary objective of simplifying, accelerating, and enhancing the development process.[8]

For end-users, programmers, and designers utilizing Flutter. Moreover, Flutter is a versatile programming language that enables the creation of a single codebase for Android, desktop, and iOS platforms. The preferred approach in this context involves leveraging the innovative Flutter framework with the Dart programming language.

THEORETICAL BACKGROUND

Mobile Applications in Healthcare:

Healthcare applications encompass various mobile apps designed to assist in various health-related tasks. These apps can range from lifestyle mHealth solutions such as fitness and meditation applications to more advanced products that heavily rely on technological advancements, like those created to aid medical professionals in diagnosing and addressing complex medical issues.[9]

In a recent publication, a comprehensive framework for a smart mobile Internet-of-Things (IoT) healthcare system was proposed to monitor patients' health risks using a smartphone and 5G technology.[10] Web and mobile applications were developed to cater to the needs of patients, doctors, laboratory analysis, and hospital services. This study used these applications to collect physiological data such as body temperature, pulse rate, and oxygen saturation levels. The physiological data were then processed using 5G technology, body sensors connected to Arduino boards, and Raspberry Pi boards.[10]

This innovative system provides real-time advice and alerts to doctors and medical assistants regarding changes in patients' vital signs and significant environmental changes. This enables medical professionals to take preventive measures swiftly, potentially saving lives in critical care and emergencies.[10]

Furthermore, mobile applications are sometimes utilized in telemedicine technologies, such as the mHealth applications operating in India as detailed in a recent study. These applications offer features like online doctor consultations or offline doctor appointment bookings, serving as an effective medium for doctor-patient communication and leading to notable enhancements in patients' health outcomes. The study involved a cross-sectional, observational, and web-based research approach.[11]

METHODOLOGY

Designing Questionnaires, Data Sorting, and Analysis

After data collection, the common issues and malfunctions identified from questionnaires and experiences with various machine types were analyzed. Subsequently, the data was categorized into four groups based on machine types, each encompassing all relevant data and malfunctions. These categories were then reviewed with the company's expert engineers to identify suitable solutions from manuals. The identified issues were then condensed and organized into four groups based on the occurrence timeline, from machine startup to disinfection before the next patient. This systematic arrangement facilitated sorting errors and the implementation of appropriate solutions, preparing them for inclusion in the codes.

Selecting the Appropriate Code Editor

Initially, the coding environment on the computer must be set up. The Android Studio and the Flutter framework were utilized as the code editor. Subsequently, the Flutter was integrated into the Android Studio, and the preferred Android version was selected; in this case, Android version 4.0.0 was chosen to ensure compatibility with devices possessing minimal specifications, thereby enabling widespread usage of the application. Constructing the Architecture of the Flutter Framework.

Constructing the Framework Architecture for Flutter

To construct a robust architecture, it is essential to incorporate a plugin for the Dart compiler, a separate plugin for code analysis, and yet another plugin for managing the Flutter developer workflow, encompassing tasks

such as building, running, and debugging. These plugins can be seamlessly integrated within Android Studio for optimal efficiency.

Creating App Widgets

The user interface (UI) and widgets utilized in the design process were carefully crafted with a harmonious color scheme and intuitive interactive features to align with the primary project objectives. The diagram in Figure (1) below showcases the app's key buttons and navigation element illustrating how users will engage with the application.

Test Execution

The Dart language continuously self-evaluates the code to detect any errors before running the application. The final evaluation of the entire code and its structure

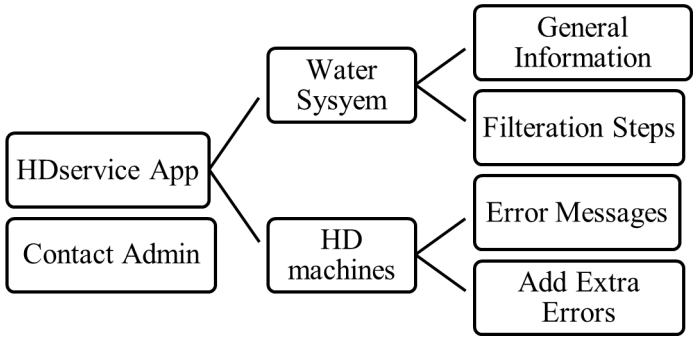

FIGURE 1. UI of the app.

is done through a specific function in the Android file named "test." This function verifies the integrity of the code even in the absence of errors.

Application Execution

Prior to launching the application, a virtual device emulator must be created on the laptop to preview the simulated app. Once everything appears satisfactory, the application is named "HDservice."

Creation of Application Icon

When developing any application, it is essential to have a unique logo that symbolizes the app's purpose. Once the logo is chosen, the image should be saved in PNG format using the website www.icongenerator.com.

APK Release

The final stage involves converting the application into APK format to make it accessible to a wider audience. The command "--release "generates two files that engineers can easily install on Android mobile devices to achieve the intended goal.

RESULTS AND DISCUSSION

The Data Obtained from the Questionnaire

The survey was completed by a cohort of 100 biomedical engineers, from which various data points were collected. These included the duration of training, ranging from one to six months, as well as the number of years of experience in the field of dialysis, as illustrated in Figure 2 below.

Moreover, the engineers encountered challenges in handling and interpreting service manuals due to several factors. To begin with, 71.1% expressed that insufficient training and workshops were provided. Additionally, 17.8% reported a lack of company engineers available for guidance and training, while 11.1% found the service manuals unclear and written in complex language.

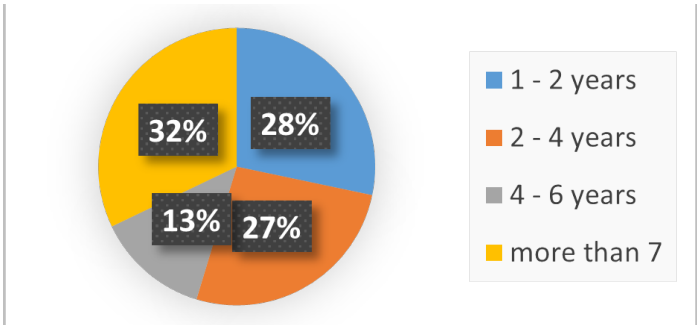

FIGURE 2. The years of experiences.

The second reason is related to the nature of the job itself. A total of 88.9% of respondents indicated no written guidelines for daily, weekly, and monthly maintenance, while 11.1% stated that such guidelines exist in their hospitals. In the event of new malfunctions, technicians typically follow a series of steps to address them, such as consulting service manuals, reaching out to colleagues,

or contacting the company's engineers. The comparison between the current procedures performed and the ideal procedures as perceived by the technicians is illustrated in Figure 3 below.

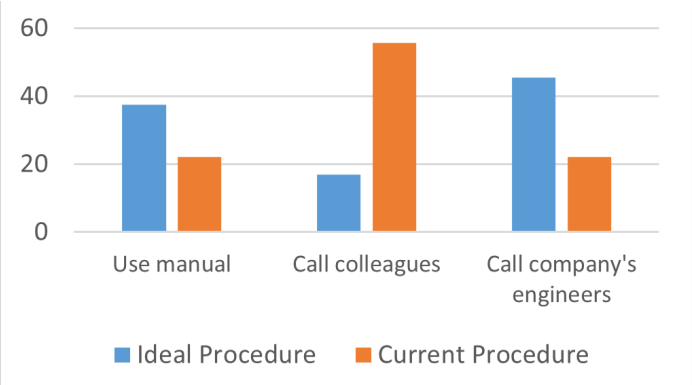

FIGURE 3. Comparison between procedures of fixing errors.

The disparity between the optimal solution and the current practice lies in the unavailability of the company's engineers due to their obligations with the vast hemodialysis centers and other responsibilities.

In line with the issue, the training workshops for engineers have proven insufficient to adequately equip them. Over the past five years, 68.2% have only attended 1–2 workshops, 25% have attended 3–4 workshops, and 6.8% have participated in more than 5 workshops.

The feasibility of the app concept was deliberated upon before its inception, with an overwhelming 89% expressing strong approval, while the remaining individuals exhibited varying degrees of disinterest.

The engineers anticipated that the app would serve as the ultimate solution during their work, with 64% endorsing this notion, marking a pivotal moment in the project's initiation.

The successful launch of the HDservice App has come to fruition.

Subsequent data will elucidate the culmination of the preceding chapter, showcasing the app post-launch to offer the desired solutions or information. Figure 4 illustrates the app's nomenclature and logo icon, epitomizing its purpose - the name conveys the provision of hemodialysis services, while the logo underscores the importance of maintaining the hemodialysis machine.

The subsequent figures will reveal the culmination of the previous chapter, displaying the app upon launch to provide the desired solution or information. Figure 4 showcases the app's name and logo icon, symbolizing the app's purpose - the name signifies the provision of hemodialysis services, while the logo conveys the importance of maintaining the hemodialysis machine.

FIGURE 4. The app's name and logo.

The application has been meticulously programmed and will continue to be enriched with new information through collaboration between my supervisor and me. It has been intricately coded to operate seamlessly offline, thus circumventing the prevalent network issues in Sudan. This design choice aims to enhance user experience for biomedical engineers, facilitating their search for errors. However, online connectivity is required for users to communicate with us, the developers, to report errors or suggest solutions for inclusion in the subsequent version. The following diagrams depict the application's process to troubleshoot and resolve various issues.

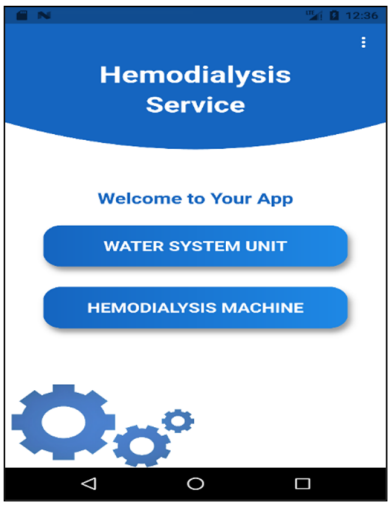

FIGURE 5. First app's screen.

The illustration depicted in Figure 5 displays the initial interface of the application, also known as the welcome screen. This screen features the app's title and a menu bar, which includes contact information as illustrated in Figure 6. The buttons in the center serve as a submenu that allows users to navigate to different screens within the app.

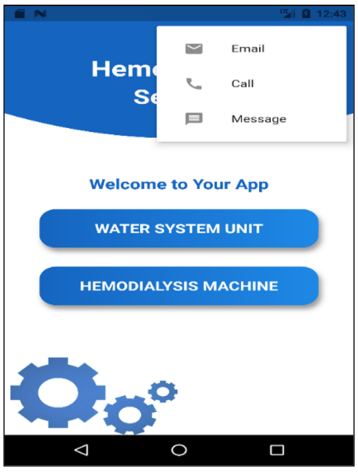

FIGURE 6. Contact information.

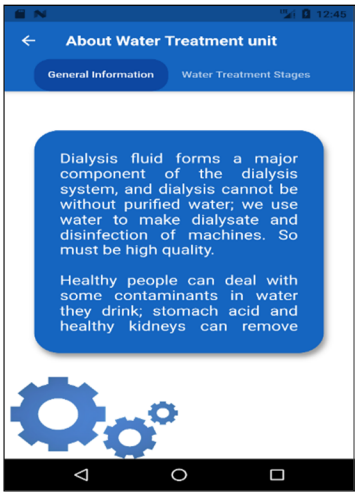

FIGURE 7. The section of water treatment unit.

The illustration above provides a comprehensive app overview and offers guidance on identifying and resolving issues. Subsequent illustrations will further elucidate this process.

For instance, if an error occurs in a BBraun machine during a self-test, the engineer must first double-click on the hemodialysis machine icon (Figure 6). Following this, the engineer should double-click the self-test button in Figure 8. Once the self-test button is double-clicked, the engineer will be directed to Figure 9 to locate the error message or code.

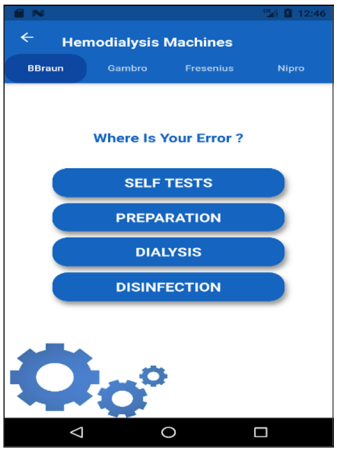

FIGURE 8. The section of HD machines.

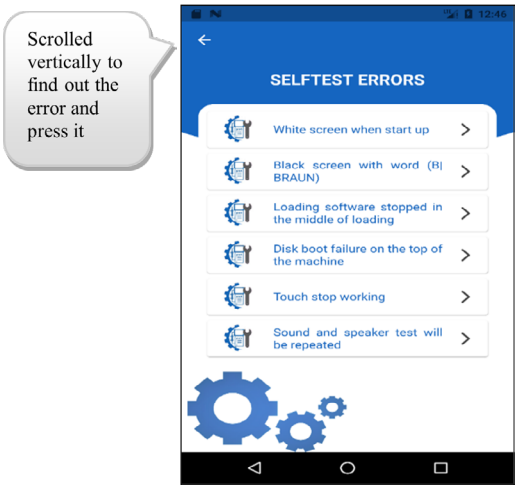

FIGURE 9. Scrolled list-view for self-test errors.

The diagram provided above displays all the errors detected during the self-test. The list-view widget was utilized to ensure that the errors can be displayed without any limitations in length, and can be expanded in the future. Each error message is represented as a widget known as a "card," which, when clicked, will navigate the user to the corresponding solution screen, as illustrated in the upcoming diagram. The solution screen depicted in Figure 10 below provides detailed explanations for why the error occurred and the potential causes behind it, this applies to all the other cards and machines as well.

FIGURE 10. The error's solution.

Assessment Feedback

Following the utilization of the application, we sought to gain a comprehensive understanding of its functionality, user satisfaction, and overall worthiness for further development. To achieve this, we conducted an online survey to assess user acceptance. The initial feedback revealed a strong acceptance rate of 89%, with the remaining responses varying between disapproval and moderate interest, as depicted in Figure 11 below. Respondents highlighted the app's user-friendly interface, which facilitated enhanced knowledge sharing and interaction between junior and senior users and provided valuable training on proper maintenance practices. This positive reception corroborated our objectives.

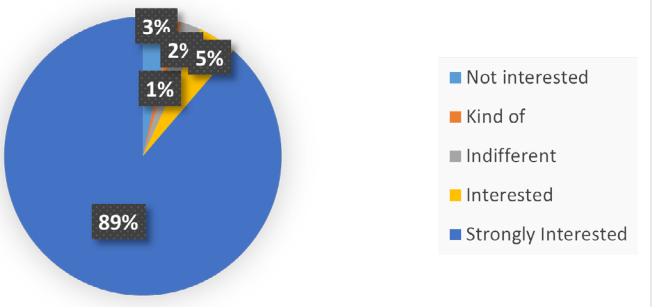

FIGURE 11. The acceptance of HDservice App.

Furthermore, the application underwent evaluation by a panel of engineers at the Military Hospital, including Eng. Salim Mohammed Musa, the chief engineer in Sudan and former technical representative of Gambro in Sudan, along with representatives from SAMASU Medical Company, the current technical agent of Gambro in Sudan.

CONCLUSIONS

The advancement of technology, particularly mobile applications in healthcare, is highlighted in this article. The mobile applications suggested here aim to offer extensive services to aid training programs and provide maintenance information for biomedical engineers regarding hemodialysis machines and water treatment systems. Using the Flutter framework to develop the app resulted in a user-friendly interface with a single code base for multiple platforms. The app's classes facilitated the easy addition of new information, serving as a foundation for knowledge sharing and experience exchange.

Employing the "HDservice app" for maintenance purposes enhances the expertise of biomedical engineers, enabling them to quickly identify the correct solutions without the need to consult colleagues. The app serves as a comprehensive guideline, akin to service manuals, thereby minimizing errors during maintenance procedures. Navigating through the app's interface to access information on different machines is swift, aiding in rapidly diagnosing malfunctions.

Furthermore, the app educates users on error solutions and fosters the sharing of experiences between seasoned engineers and novices. The authors will regularly update the app with new information based on user submissions, promoting continuous learning. The increasing integration of mobile applications in healthcare is anticipated, with this app serving as a pioneering platform for developing apps for other medical instruments.

ACKNOWLEDGMENT

I sincerely appreciate individuals who contributed to this project, particularly in the programming aspect, from inception: Eng. Alaa Yahia, Albaraa Omer, and a special

thank you to Eng. Jabir Mohammed for his invaluable time, guidance, and advice.

I express immense thanks and acknowledgment to the engineers who provided information on dialysis machines: Motasim Almamoun, Eman Tag Alsir, and Yousif Mohammed. Additionally, I appreciate the support and encouragement from my colleagues and friends at Alnaw and Algazira Slang Hospitals for Kidney Diseases.

REFERENCES

1. Medical Education Institute. Core Curriculum for the Dialysis Technician. A Comprehensive Review of Hemodialysis. 5th edition. Author; Madison, WI.
2. Ward RA, Ronco C. Dialyzer and Machine Technologies: Application of Recent Advances to Clinical Practice. Blood Purification. 2006.
3. Hamza AO, Osman MO, Khider MO. Evaluation of Mechanical and Electrical Faults in Dialysis Machines. J Phys Ther Health Promot 2013;1(1):1–7.
4. Sheikh Z. When Do I Need Dialysis. [Internet] Available at: https://www.webmd.com/a-to-z-guides/kidney-dialysis.
5. Naramura T. The role of clinical engineers in dialysis therapy in Japan. Blood Purification 2018;46:134–135.
6. Misra KB. Maintenance Engineering and Maintainability: An Introduction. RAMS Consultants. Jaipur, India. August 2008.
7. World Health Organization. Computerized Maintenance Management System. WHO Medical device technical series. Geneva. June 2011.
8. Mainkar P, Giordano S. Google Flutter Mobile Development Quick Start Guide. Packt Publishing, Birmingham Mumbai, 2019. Available at: https://www.studypool.com/documents/19492261/google-flutter-mobile-development-quick-start-guide-prajyot-mainkar-salvatore-giordano-https://shakuro.com/blog/healthcare-mobile-app-development-why-how-and-how-much.
9. Nasri F, Mtibaa A. Smart Mobile Healthcare System based on WBSN and 5G. Int J Adv Comp Sci Applicat 2017;(8)10. Available in at: DOI:10.14569/IJACSA.2017.081020 .
10. Agarwal N, Biswas B. Doctor Consultation through Mobile Applications in India: An Overview, Challenges and the Way Forward. Healthcare Informatics Research. Available at: https://doi.org/10.4258/hir.2020.26.2.153pISSN 2093-3681

Received May 17, 2024, accepted June 25 2024, date of publication July 10 2024.

Comparative Performance of Low-Cost Portable Scanner in Pregnancy Profile Ultrasonography: A Promising Adjunct to Telemedicine

By Afroza Naznin[1,2], Muhammad Abdul Kadir[1], Fatima Begum[3], Khondkar Siddique-e Rabbani[1]

[1] Department of Biomedical Physics and Technology, University of Dhaka, Dhaka 1000, Bangladesh

[2] Institute of Nuclear Medicine & Allied Sciences, Sir Salimullah Medical College & Mitford Hospital, Bangladesh Atomic Energy Commission, Dhaka, Bangladesh

[3] National Institute of Nuclear Medicine & Allied Sciences, Bangladesh Atomic Energy Commission, Dhaka, Bangladesh

ABSTRACT

Background and Objective: Ultrasound scanners are widely used in various clinical settings, but conventional devices are too expensive to deploy in every healthcare facility in low-resource countries. Alternative, less costly instruments with comparable efficacy are required to ensure this diagnostic service is available in even remotest areas. This study evaluated the effectiveness of a commercially available low-cost portable ultrasound machine, particularly focusing on pregnancy profiling.

Material and Methods: A total of 77 pregnant females were scanned for basic obstetric parameters with two devices, first the low-cost scanner, and then a conventional ultrasound machine, considering the latter as the gold standard. The key obstetric parameters observed were the number of fetuses, the presence of cardiac pulsation and fetal movement, fetal biometry including Crown Rump Length (CRL), Bi-Parietal Diameter (BPD), and Femoral Length (FL), gestational age, placental location, amniotic fluid volume, and presentation of the fetus.

Results: The portable device performed well compared with the standard machine in observing the fetal number, presentation, movement, heartbeat, placental location, and amniotic fluid volume. The correlation coefficients (r^2) for measuring BPD, FL, CRL, and gestational age using the portable and standard devices were 0.9578, 0.9415, 0.8230, and 0.983, respectively. The mean absolute error (MAE) in the measurement of BPD, FL, CRL, and gestational age were 2.24 mm, 2.14 mm, 6.5 mm, and 0.94 weeks, respectively.

Conclusion: The results demonstrated the potential of low-cost portable ultrasound devices in pregnancy profile scanning. Further studies with larger sample sizes are needed to explore their full potential. With appropriate data transfer arrangements, these devices have significant potential for integration into telemedicine services.

Keywords – *Portable ultrasound, Antenatal care, Pregnancy profiling, Maternal health, Telemedicine.*

INTRODUCTION

Ultrasonography (USG) is a non-invasive clinical imaging modality that has gained widespread acceptance as a reliable diagnostic tool. It requires less infrastructure and logistic support than instruments used for X-ray examinations, computed tomography, or magnetic resonance imaging, but it provides real-time information. This technology has found its way into various clinical settings, including gynecology and obstetrics. The acceptability of USG is more profound in this specialty due to a lower radiation hazard. Pregnant women are recommended to have at least one USG scan during the antenatal period to estimate gestational age, and improve detection of fetal anomalies and multiple pregnancies.[1]

Maternal mortality rate is variable in different parts of the world reflecting inequalities in economic conditions and quality healthcare access. In 2020, around 95% of all maternal deaths occurred in low and lower-middle-income countries, which was 430 per 100,000 live births.[2] However, the sustainable development goal target is to reduce maternal mortality to less than 70 per 100,000 live births by 2030. Most of these deaths are due to preventable causes, so early detection of complications is crucial to ensure prompt clinical intervention, which can be lifesaving. Pregnancy complications also have long-term effects on maternal health.[3] Therefore, implementing USG in remote healthcare facilities for expecting mothers should be urgently considered. However, USG devices are costly and not readily accessible to rural populations, especially in low-income countries.[4]

Currently, tablet- or smartphone-based portable USG scanners are available at relatively low prices.[5] Portable USG allows healthcare providers to conduct real-time ultrasound examinations remotely. Through telemedicine platforms, clinicians can guide on-site healthcare workers or patients to perform ultrasound scans, providing valuable insights. Portable ultrasound devices are particularly valuable in low-resource settings, such as rural areas or underserved communities, where access to advanced medical facilities is limited. Telemedicine can bridge the gap by connecting local healthcare providers with specialists who can remotely interpret ultrasound images. In obstetrics, portable USG in telemedicine can support prenatal care. Expectant mothers can undergo ultrasound scans locally, with the results transmitted to specialists for analysis. This approach ensures that pregnant women in remote areas receive timely and expert guidance throughout their pregnancy. Therefore, implementing USG in remote healthcare facilities for expecting mothers should be urgently considered.

However, USG devices are very expensive and not readily accessible to rural populations in low-income countries.[4] Currently, tablet- or smartphone-based portable USG scanners are available at relatively lower prices.[5] However, the utility of such low-cost portable scanners in pregnancy profiling must be investigated before deployment in any healthcare program.[6] Heuvel et al. conducted a comparative analysis assessing the efficacy of low-cost ultrasound devices for estimating gestational age (GA) in resource-limited settings, suggesting the feasibility of utilizing such devices for GA estimation.[7] Stock et al. compared the performance of pocket-sized ultrasound device with a premium machine in bedside examinations and reported limited utility.[8] Bruns et al. explored the suitability of pocket ultrasound as a supplementary tool for clinical assessment specifically during the first trimester of pregnancy.[9] Kodaira et al. conducted a study to evaluate the reliability of ultrasound findings acquired through handheld devices in urgent obstetric scenarios, reporting good agreement ($\kappa > 0.8$) particularly concerning fetal number, presentation, and heartbeat.[10] In another study focusing on routine antenatal third-trimester ultrasonography, researchers found substantial concordance between a pocket-sized USG machine and high-specification USG units regarding fetal presentation and development.[11] This study involved the scanning of 51 patients, concluding that portable devices are accurate tools for assessing various parameters, including fetal number, presentation, placental site, amniotic fluid volume, and the presence of key structures during the third trimester of pregnancy. However, prior studies primarily examined specific trimesters or focused on a limited number of obstetric parameters. Thus, the present study aims to investigate a comprehensive range of obstetric parameters across all three trimesters of pregnancy.

MATERIALS AND METHODS

Study design

This was a cross-sectional study conducted from June 2022 to December 2022. A total of 77 subjects were randomly selected from female patients who came to the hospital for pregnancy profiling with more than eight weeks of gestation according to their menstrual history. Pregnant patients with any emergency or life-threatening condition such as pervaginal bleeding, eclampsia, pre-eclampsia, premature rupture of membrane, severe abdominal pain, etc., or those who were in any stage of active labor were excluded. For a significance level of 0.05, a power of 80%, and a disagreement probability of 0.5, the sample size required to detect a Cohen's kappa value of 0.90 is 73.[12] The disagreement rate of 0.5 was chosen because it represents the midpoint where the sample size is the highest. Therefore, this study's sample size of 77 subjects can be considered statistically significant. The number of subjects in the first, second, and third trimesters of pregnancy was 3, 15, and 59, respectively. This study did not consider pregnancy cases earlier than 8 weeks to avoid potential hazards from ultrasound energy. This exclusion criterion explains the lower number of cases in the first trimester.

Ethical statement

This study was conducted under the principles embodied This study was conducted under the principles embodied in the Declaration of Helsinki and in accordance with local statutory requirements. Necessary ethical approval was obtained from the National Research Ethics Committee, Bangladesh (No: 45713122021) for this study. Informed consents were obtained from all participants.

Data collection

After receiving informed consent, each patient was scanned twice: first, with a low-cost tablet PC-based portable and hand-held device, and then with a sophisticated and expensive scanner by a sonographer. Adequate time interval was given between the two scans to avoid bias. The portable USG device (Sunbright P1), which comprises a wired probe (frequency 3–5 MHz, depth 24 cm), is connected to a smartphone or computer.[13] The portable device was chosen considering its low cost, commercial availability, safety (CE [Conformité Européenne] certified), and data transfer ability to PC and smartphones. Data from the portable device was tested against a sophisticated and expensive machine (Samsung Medison Accuvix A30), conventionally used in hospital settings, which is an USG system with a 21.5-inch-wide LED monitor (screen resolution 1920 × 1080) and four probes (depth 2–30 cm).[14] The frequency range of the convex probe of the conventional device used for this study was 2–6 MHz. This sophisticated machine's output was considered gold standard for comparison of the portable scanner mentioned above. However, the actual measurements taken of any imaged organ depend on the personal choice of selected points on the image by the sonologist, so there would be errors in the gold standard too. Therefore, this has to be kept in mind when comparing the performance of the portable device with that of the standard device.

The key obstetric parameters observed were:

(i.) Number of fetuses
(ii.) Presence of cardiac pulsation and fetal movement
(iii.) Fetal biometry including CRL, for first-trimester pregnancies
(iv.) BPD and FL, beyond the first trimester
(v.) GA
(vi.) Placental location
(vii.) Amniotic fluid volume
(viii.) Presentation of the fetus

Images captured on the portable device were saved and subsequently transferred to a computer to measure these obstetric parameters. Information was also recorded in a tabulated form. Diameters and lengths were measured using electronic calipers. CRL was measured from the top of the head (crown) to the bottom of the buttocks (rump) of the fetus. BPD was measured from the outer edge of the near calvarial wall to the inner edge of the far calvarial wall. FL was identified as the measurement of longest bright echo within the fetal femur. All measurements were taken three times, and the arithmetic mean was recorded for analysis.

Analysis and presentation

Firstly, the values of each parameter obtained using the portable device were plotted against the corresponding values obtained using the standard device to observe whether an overall correlation exists or not. The agreement between the two devices regarding categorical variables was assessed with Cohen's kappa value. If the value is within 0.61–0.8, it denotes substantial agreement while values above 0.8 (maximum possible: 1.00) represent almost perfect agreement.[15] For continuous variables, Bland-Altman plot and paired t-test were applied. Statistical analyses were performed using SPSS software and Microsoft Excel. The Bland-Altman diagram is a statistical method that offers insight into the pattern and extent of any agreement. To draw the diagram, the difference between a pair is plotted on the vertical axis of the diagram against the mean of the pair on the horizontal axis. The upper and lower limits of the interval shows the limits of agreement; then it is decided subjectively whether the agreement between pairs of readings is acceptable.[16]

To evaluate the performance of the portable device, mean absolute error (MAE) was also calculated using equation (1).

$$MAE = \frac{\sum_{i=1}^{n} |X_{port} - X_{conv}|}{n} \quad (1)$$

Here, X_{port} is the obstetric parameter measured by the portable device, X_{conv} is the corresponding parameter measured by the conventional (standard) device and n is the number of subjects.

RESULTS

The total number of pregnant females was 77, aged 18 to 35 years with a mean age of (25.8 ± 4.27) years. The obstetric parameters we have focused on in this study are the number and presentation of fetus, presence of cardiac pulsation and fetal movement, fetal biometry (CRL, BPD and FL), estimation of GA, placental location, and amniotic fluid volume. Figures 1 to 5 present a selection of ultrasound images obtained using both conventional and portable devices, providing a representative overview of the typical study results. Notably, the images captured by the low-cost portable device exhibit lower resolution, resulting in inferior image quality and a lack of detail in smaller tissue areas.

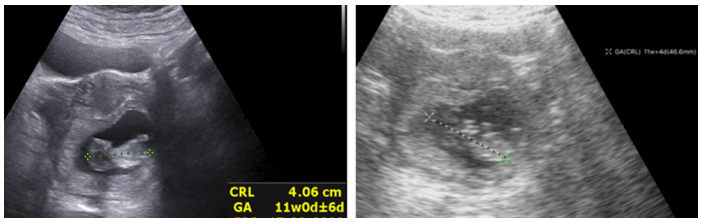

FIGURE 1. Figure 1. Ultrasound scan images of a first trimester fetal pole for Crown Rump Length (CRL) measurement taken with the standard device (left) and with the portable device (right)..

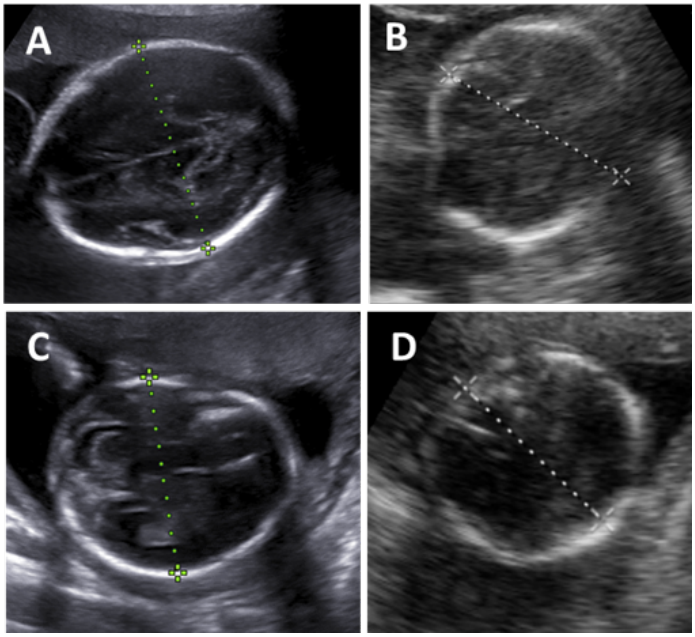

FIGURE 2. Figure 2. Ultrasound images of two second-trimester fetal heads captured using standard device (A, C) and portable device (B, D).

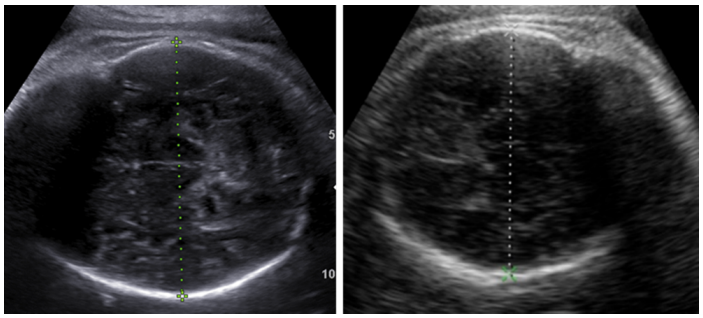

FIGURE 3. Ultrasound images of a third-trimester fetal head for Bi-Parietal Diameter (BPD) measurement captured with standard device (left) and portable device (right).

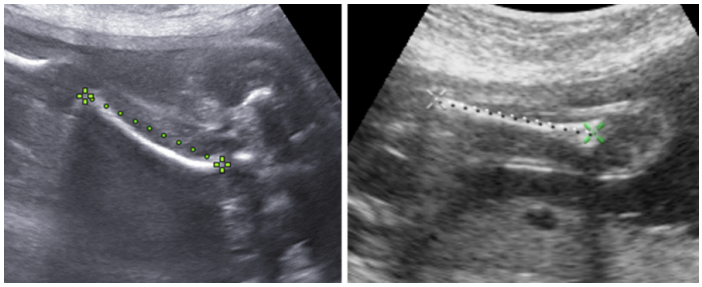

FIGURE 4. Ultrasound images of a second-trimester fetal femur recorded with standard device (left) and portable device (right).

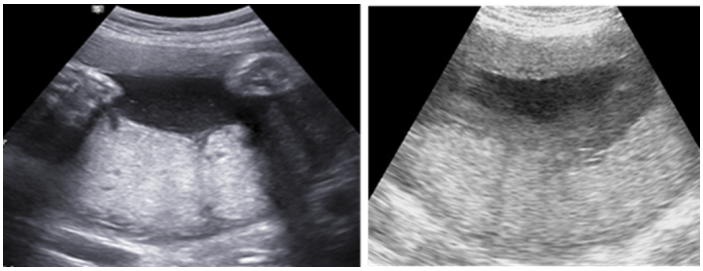

FIGURE 5. Ultrasound images of a placenta, with the left image captured by the standard device and the right image obtained using the portable device.

Figure 1 illustrates images of a first-trimester fetal pole intended for CRL measurement. The image on the left, taken with the standard device, demonstrates a clearer and more defined fetal pole compared to the image on the right, captured by the portable device. The fetal outline appears less distinct in the portable device's image, highlighting the difference in image clarity between the two scanners.

Figure 2 presents ultrasound scan images of two second-trimester fetal heads captured using both devices. Specifically, Figure 2A and Figure 2C display images obtained from the conventional device, while Figure 2B and Figure 2D depict the corresponding scans acquired with the low-cost portable device. The cross marks in the images indicate specific points identified by the sonologist for precise measurements along the marked dotted lines. Moving on to Figure 3, ultrasound scan images of a third-trimester fetal head for BPD measurement are showcased. The image on the right is obtained from the portable device, while the left image is captured using the conventional unit. Although not precisely identical, the image quality and details are considerably similar between the two.

In Figure 4, ultrasound scan images of a second-trimester fetal femur are presented, with the left image taken using the standard device and the right image with the portable device. Figure 5 displays ultrasound images of a placenta, with the left image captured by the standard device and the right image obtained using the portable device. Notably, the echogenic layer adjacent to the anterior wall in the right-hand image exhibits a reverberation artifact, which is exaggerated compared to the left-hand image.

Correlation of measured values

Figure 6 shows a scatter plot for BPD with the values obtained using the portable device plotted against that obtained using the standard device. The linear correlation is very high with a squared correlation coefficient (r^2) of 0.9578. The slope is about 0.98, which is close to 1, meaning that the two values are almost identical.

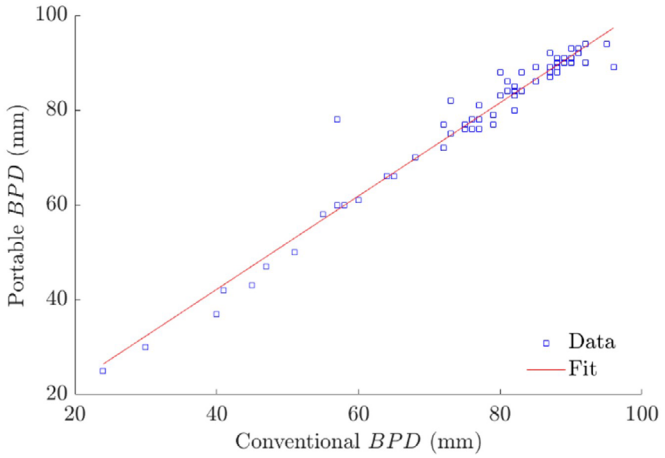

FIGURE 6. Scatter plot showing correlation between BPD measurements taken with two devices.

In order to compare the two sets of values in more detail, a Bland-Altman plot is shown in Figure 7. For these plots, the values obtained using the conventional device (the gold standard here) were subtracted from the corresponding ones obtained using the portable device for each subject and plotted along the vertical axis. The means of the BPD values for each subject obtained using both the devices were plotted along the horizontal axis. It shows that the portable device tended to underestimate BPD in earlier pregnancies, while the deviations became less as the fetal size increased. Overall the mean value of BPD given by the portable device was 1.6 mm greater than

those obtained using the conventional device. The plot also shows that 95% of the portable device measurements remained within +8 mm and −5 mm range of the actual values. The MAE for measuring BPD using the portable device was 2.24 mm.

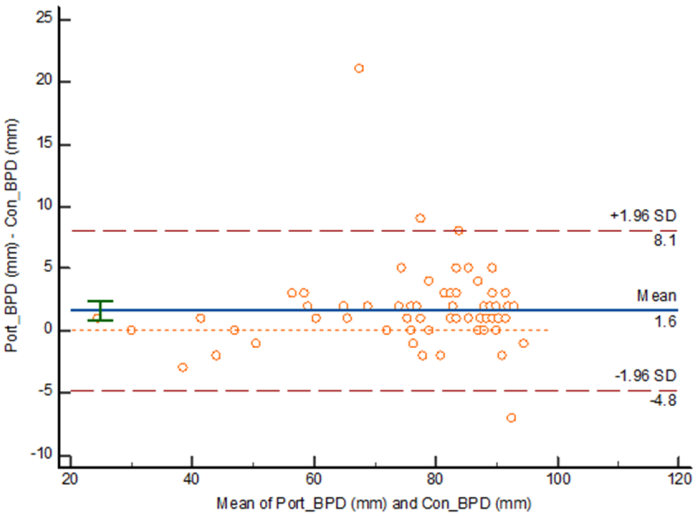

FIGURE 7. The Bland-Altman plot shows the difference of the two paired BPD measurements plotted against the mean of the two measurements.

Figure 8 shows the correlation (r^2=0.9415) between FL measurements taken with two devices. There was no tendency towards under or overestimation in relation to GA, and 95% of the measurements fell within the range +6.2 mm to −7.2 mm, the mean being at −0.5 mm (Figure 9). The MAE in measuring FL was 2.14 mm.

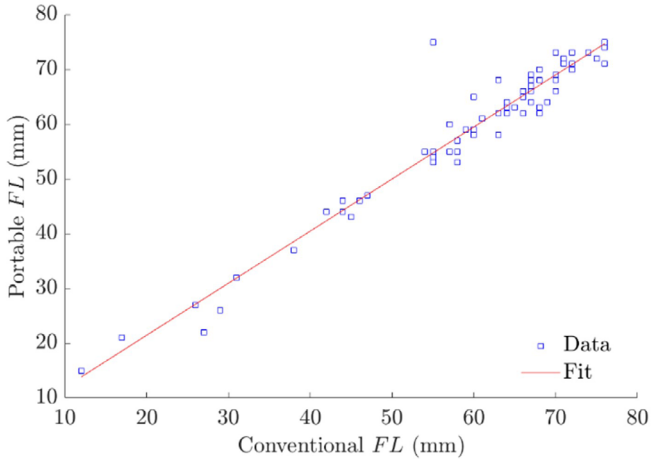

FIGURE 8. Scatter plot showing correlation between FL measurements taken with two devices.

The portable machine produced wide variations for CRL measurements, about 9 to 17 mm from actual values (Figure 10). The correlation between the two devices in measuring CRL is relatively low (r^2=0.823) as shown in Figure 11. The MAE in measuring CRL was found to be 6.5 mm.

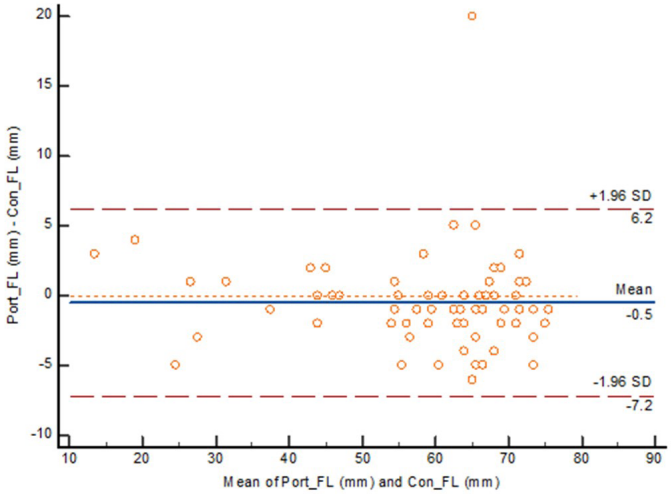

FIGURE 9. The Bland-Altman plot shows the difference of the two paired FL measurements plotted against the mean of the two measurements.

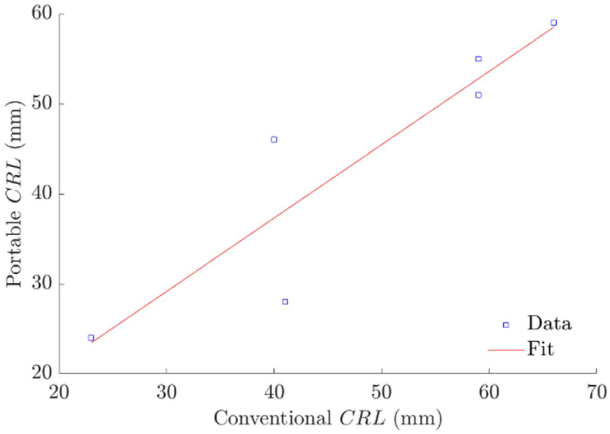

FIGURE 10. Scatter plot showing correlation between CRL measurements taken with two devices.

In case of GA estimation, out of 77 pregnancies, three were in the first trimester i.e., below 12 weeks, 15 in the second trimester (12–26 weeks) and 59 cases were in the third trimester (beyond 26 weeks), as determined by the conventional USG machine. Figure 12 shows the correlation (r^2=0.983) between FL measurements taken

with two devices. Bland-Altman plot in Figure 13 showed 95% of the values taken with the portable scanner to be within almost two two-week range of the actual values. The MAE in measuring GA was 0.93 weeks. It was also noted that GA was mostly underestimated by the low-cost device in first and second-trimester pregnancies, up to around 32 weeks of gestation; whether towards term pregnancies, it was more overestimated. Again, the percentage of deviation of the GA measured using the portable device decreased as the GA increased.

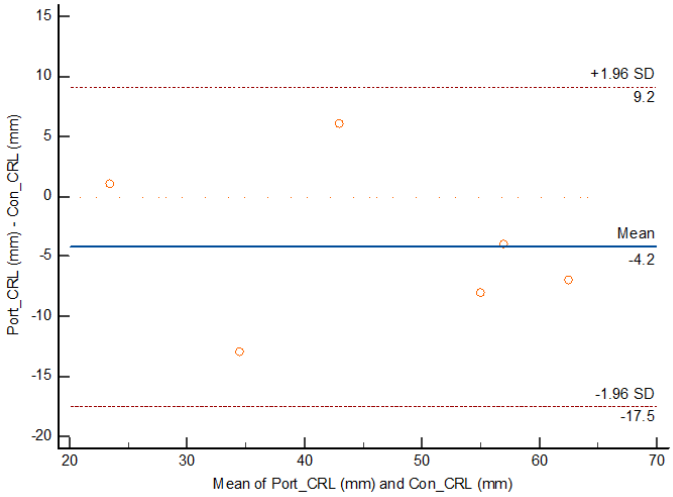

FIGURE 11. The Bland-Altman plot showing wide variations in CRL measurements from the two devices.

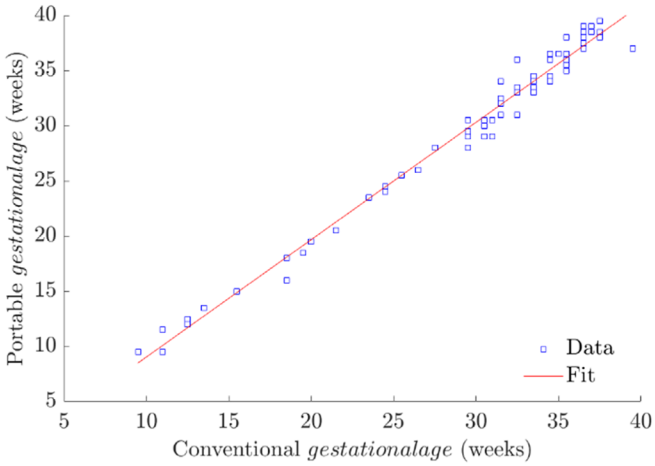

FIGURE 12. Scatter plot showing correlation between gestational age measurements taken with two devices.

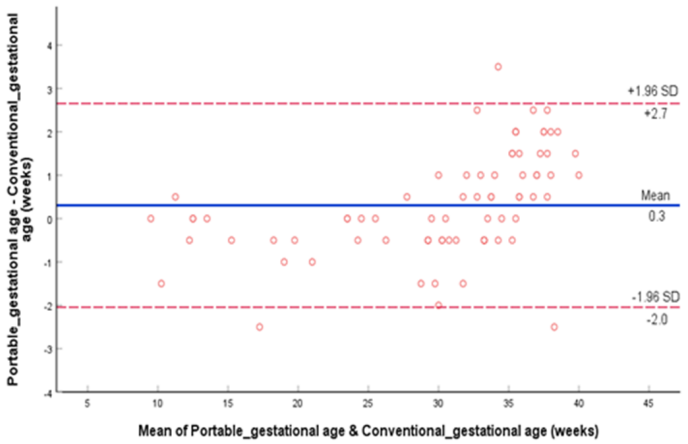

FIGURE 13. The Bland-Altman plot where the difference of the two paired gestational age measurements is plotted against the mean of the two measurements.

Other parameters

This study had five qualitative variables: presentation, the fetus's movement and heartbeat, placental location and amniotic fluid volume. Majority of the fetus was in cephalic presentation (80.5%), followed by floating condition (15.6%) and breech (3.9%). Fetal movement was present in about 94.8% of the cases, with 3.9% being too early to comment and one case where movement was absent. We found 76 live pregnancies with regular cardiac pulsation and one case of intra-uterine death. Regarding placental location, in most cases, it was found in anterior uterine wall (53.2%), followed by posterior wall (29.9%). Fundal, anterofundal and posteriofundal locations were less common. In about 93.5% cases amniotic fluid volume was adequate, with 3.9% cases of oligohydramnios, and 1.3% cases of polyhydramnios. The portable machine's findings agreed with the standard device (Table 1). Chi square test also showed significant result (P value < 0.001).

Single or Multiple pregnancies

By scanning with the conventional USG machine, which was considered as the gold standard, 72 cases were found to have single pregnancy, while 4 cases had twin pregnancy and one case had a triplet. The portable device could detect a number of fetus accurately in all these cases.

TABLE 1. Kappa Values for Qualitative Variables Showing Good Agreement between Two Devices

Parameter	κ statistic	P value	Interpretation
Fetal presentation	1.0	< 0.001	Perfect agreement
Fetal movement	1.0	< 0.001	Perfect agreement
Fetal heartbeat	1.0	< 0.001	Perfect agreement
Placental location	0.892	< 0.001	Very good agreement
Amniotic fluid volume	0.884	< 0.001	Very good agreement

DISCUSSION

Portable USG scanner, by virtue of its affordability and mobility, is being contemplated for use in different low-resource settings like refugee camps, remote villages, etc. besides general practice.[17–19] This study compared the performance of a low-cost portable ultrasound scanning device to a more expensive standard device, particularly for obstetric parameters. Very good agreement between the two devices in measuring most of the parameters was observed in this study, which are number and presentation of fetus, presence of cardiac pulsation and fetal movement, fetal biometry (CRL, Bi-Parietal Diameter, FL), estimation of GA, placental location, and amniotic fluid volume. However, CRL had more deviation as this was measured in the first trimester when the fetus was small, and marking out points with the low-cost portable device was challenging because of lower resolution. However, as the fetus increased, the errors in all parameters decreased and were within tolerable limits for acceptance.

GA was determined by measuring fetal biometry; CRL in first-trimester pregnancies, and BPD, FL in second and third trimesters. Sac diameter is another measure for GA determination in earliest pregnancies, but it was not used as this study only enrolled pregnant females with more than eight weeks of gestation.[20] Regarding CRL estimation, first-trimester fetal poles are very small, and it might be difficult for a low-resolution probe to outline the full length separately from yolk sac and inner wall of sac (see Figure 1). However, a positive linear correlation was observed between CRL values of both devices with r^2 higher than 0.8 (see Figure 10). The relationship with fetal size could be appreciated in the Bland-Altman plot, which shows that despite the variable discrepancy, deviation from reference value decreased as CRL approached 55 mm and higher (see Figure 11). Very few first trimester cases were included in this study, which was inadequate to reach any definite consensus regarding the efficacy of CRL measurement. A Norwegian study focused exclusively on hand-held trans-abdominal ultrasound's ability to evaluate first-trimester viable intra-uterine pregnancy.[21] They investigated 100 women, comparing hand-held device findings to that of high-end trans-vaginal USG. According to their observation, viability could be confirmed with 79% positive and 100% negative predictive value from 7th week of gestation, and CRL measurements were comparable with a median difference of 1 mm. Of course, the error also depends on the image's resolution quality, and values obtained using one low-cost device may not apply to another device obtained from another manufacturer.

This study observed strong positive linear correlation between BPD, FL and GA measurements taken with both devices, r^2 being greater than 0.9 in all three cases (see Figures 6, 8, and 12). In a detailed assessment, the low-cost device usually underestimated BPD measurements in earlier pregnancies, up to about 58 mm, corresponding to nearly 24 weeks of gestation (see Figure 7). For the next 14–15 mm (up to around 30 weeks) portable device values were very close to standard ones, and after that deviation increased but uniformly. Figure 2 shows scan images of two fetal heads in second trimester. Both near and far calvarial walls are well outlined in the images from conventional machine, but in the portable device scans walls appear blurred, leading to incorrect estimation of BPD. This is because the hand-held scanner cannot capture relatively fast-moving fetuses of earlier pregnancies as accurately as the conventional machine. Accordingly, image quality improves when fetal size increases and the fetus is less mobile (see Figure 3).

In case of FL measurement by the low-cost instrument, there was no notable tendency towards over or under-estimation (see Figure 9). Deviation from standard was minimal between a range of approximately 30–50 mm (corresponding GA about 19–26 weeks), and beyond second trimester there was uniform increase.

Most of the portable scanner calculations of GA are within two two-week range of actual values (see Figure 13). The Bland-Altman plot shows that the difference mostly lies between one week ranges for about up to 30 weeks of gestation, and then increases gradually. It is highest between 35 and 40 weeks. This might be considered clinically acceptable because, for GA measurement by USG, it has been studied and found that parameters like BPD and FL are less accurate during last weeks of pregnancy. According to Macgregor et al. the accuracy of gestational sac measurement as a predictor of GA is approximately ±1 week. In case of CRL, the accuracy is within ±5 to 7 days. During 12–26 weeks, GA determination by BPD and FL measurements falls within a range of 10–11 days and 10–20 days respectively, for 95% of the cases. After 26 weeks, this range extends to 2–3 weeks.[22]

Fetal number, movement, presentation and cardiac pulsation were accurately detected by the portable device in all of the cases, which denotes the perfect efficacy of this instrument for assessing those parameters in more than eight weeks of gestation (see Table 1). An eight-week embryo reaches considerable development by completing organogenesis, therefore these parameters were all discernible despite low resolution. Earlier pregnancies were beyond the scope of this study to avoid potential hazard by ultrasound energy.[19] Kodaira et al. performed a study to assess the reliability of ultrasound findings acquired with hand-held apparatuses in urgent obstetric settings. They reported high agreement ($\kappa > 0.8$) in the case of fetal number, presentation and heartbeat.[10] Their overall diagnostic accuracy was still lower than ours, probably because they included emergency obstetric patients of any GA in a high volume low-resource setting, and scans were obtained by medical students with limited training.

Placenta is identified in ultrasound examination as a mostly uniform echogenic structure along uterine wall.[23] In our study, anteriorly placed placenta was the commonest location, followed by posterior; in accordance with a large population based cohort study in Sweden involving more than 74 thousand pregnant females.[24] A few fundal placentas were identified as anterior in location by the low-cost device, due to exaggeration of reverberation artifact along the anterior wall (see Figure 5). The same phenomenon might have contributed to the underestimation of amniotic fluid volume in one case of polyhydramnios. However, despite these few exceptions, the portable device showed very good agreement with the conventional machine regarding both placental localization and amniotic fluid estimation (see Table 1).

LIMITATIONS

The study was conducted with a relatively small sample size, as a result there was not enough patients from each trimester. First-trimester subjects were especially scarce, as we could not enroll females with less than eight weeks of gestation. Besides, only stable pregnant women were enlisted for study, limiting the number and varieties of pathology that could be observed. Therefore, efficacy of the portable device in emergency conditions could not be evaluated. Further study with larger sample size must be done to explore its full potential.

CONCLUSIONS

The portable device used in this study showed remarkable efficacy in observing several obstetric parameters, namely fetal number, presentation, movement, heartbeat, placental location and amniotic fluid volume. Regarding other variables, the low-cost scanner measurements were closest to gold standard during 24–30 weeks for BPD and 19–26 weeks for FL. GA determination remains within one week range from the standard reference during second trimester and first six weeks of third trimester. Observing the above-mentioned efficiency, such portable device may be recommended to provide diagnostic service in remote areas, including refugee camps, hilly areas, and islands. There is significant potential for integrating low-cost and portable ultrasound scanning devices into telemedicine service systems with appropriate data transfer arrangements. However, further studies are needed to investigate interpersonal variability in the use of portable devices, ensuring consistency and accuracy across different users and settings.

CONFLICT OF INTEREST

The authors declare no conflict of interest.

GRANT SUPPORT

The International Science Programme (ISP), Uppsala University, Sweden, is acknowledged for financial support as research grant.

REFERENCES

1. WHO Recommendations on Antenatal Care for a Positive Pregnancy Experience 2016 [cited 2024 15 March]. Available from: https://pubmed.ncbi.nlm.nih.gov/28079998/.
2. WHO. Maternal Mortality 2023 [cited 2024 15 March]. Available from: https://www.who.int/news-room/fact-sheets/detail/maternal-mortality.
3. Neiger R. Long-term effects of pregnancy complications on maternal health: a review. J Clin Med. 2017;6(8):76. https://doi.org/10.3390%2Fjcm6080076
4. Seffah JD, Adanu RM. Obstetric ultrasonography in low-income countries. Clin Obstet Gynecol. 2009;52(2):250-5. https://doi.org/10.1097/grf.0b013e3181a4c2d5
5. Rykkje A, Carlsen J, Nielsen M. Hand-held ultrasound devices compared with high-end ultrasound systems: a systematic review. Diagnostics (Basel). 2019; 9 (2):61. https://doi.org/10.3390/diagnostics9020061
6. Becker DM, Tafoya CA, Becker SL, Kruger GH, Tafoya MJ, Becker TK. The use of portable ultrasound devices in low-and middle-income countries: a systematic review of the literature. Tropic Med Int Health. 2016;21(3):294-311. https://doi.org/10.1111/tmi.12657
7. van den Heuvel TLA, de Bruijn D, Moens-van de Moesdijk D, Beverdam A, van Ginneken B, de Korte CL. Comparison study of low-cost ultrasound devices for estimation of gestational age in resource-limited countries. Ultrasound Med Biol. 2018;44(11):2250-60. https://doi.org/10.1016/j.ultrasmedbio.2018.05.023
8. Stock KF, Klein B, Steubl D, Lersch C, Heemann U, Wagenpfeil S, et al. Comparison of a pocket-size ultrasound device with a premium ultrasound machine: diagnostic value and time required in bedside ultrasound examination. Abdom Imag. 2015;40:2861-6. https://doi.org/10.1007/s00261-015-0406-z
9. Bruns RF, Menegatti CM, Martins WP, Júnior EA. Applicability of pocket ultrasound during the first trimester of pregnancy. Medical Ultrasonography. 2015;17(3):284-8. https://doi.org/10.11152/mu.2013.2066.173.rfb
10. Kodaira Y, Pisani L, Boyle S, Olumide S, Orsi M, Adeniji AO, et al. Reliability of ultrasound findings acquired with hand-held apparatuses to inform urgent obstetric diagnosis in a high-volume resource-limited setting. Internat J Gynecol Obstet. 2021;153(2):280-6. https://doi.org/10.1002/ijgo.13475
11. Galjaard S, Baeck S, Ameye L, Bourne T, Timmerman D, Devlieger R. Use of a pocket-sized ultrasound machine (PUM) for routine examinations in the third trimester of pregnancy. Ultrasound Obstet Gynecol. 2014;44(1):64-8. https://doi.org/10.1002/uog.13285
12. Temel G, Erdogan S. Determining the sample size in agreement studies. Marmara Med J. 2017;30(2):101-112. https://doi.org/10.5472/marumj.344822
13. Sunbright SUN P1 2024 [cited 2024 15 March]. Available from: https://www.sunbright.shop/Factory-price-SUN-P1-type-C-portable-usb-probes-ultrasound-for-sale-8317?d=2.11
14. Samsung. Accuvix A30 2024 [cited 2024 15 March]. Available from: https://www.samsung.com/hk_en/support/model/USS-AV30F4U/WR/
15. Barton B, Peat J. Medical statistics: A guide to SPSS, data analysis and critical appraisal: John Wiley & Sons; 2014.
16. Watson P, Petrie A. Method agreement analysis: a review of correct methodology. Theriogenology. 2010;73(9):1167-79. https://doi.org/10.1016/j.theriogenology.2010.01.003
17. Andersen CA, Holden S, Vela J, Rathleff MS, Jensen MB. Point-of-care ultrasound in general practice: a systematic review. Ann Fam Med. 2019;17(1):61-9. https://doi.org/10.1370/afm.2330
18. Løkkegaard T, Todsen T, Nayahangan LJ, Andersen CA, Jensen MB, Konge L. Point-of-care ultrasound for general practitioners: a systematic needs assessment. Scand J Primary Health Care. 2020;38(1):3-11. https://doi.org/10.1080/02813432.2020.1711572
19. Reynolds TA, Amato S, Kulola I, Chen C-JJ, Mfinanga J, Sawe HR. Impact of point-of-care ultrasound on clinical

decision-making at an urban emergency department in Tanzania. PloS One. 2018;13(4):e0194774. https://doi.org/10.1371/journal.pone.0194774

20. Van den Hof MC. No. 359-Obstetric Ultrasound Biological Effects and Safety. J Obstet Gynaecol Can. 2018:40(5):627-32. https://doi.org/10.1016/j.jogc.2017.11.023

21. Pedersen JK, Sira C, Trovik J. Hand-held transabdominal ultrasound, after limited training, may confirm first trimester viable intrauterine pregnancy: a prospective cohort study. Scand J Primary Health Care. 2021;39(2):123-30. https://doi.org/10.1080/02813432.2021.1910643

22. MacGregor SN, Sabbagha RE. Assessment of Gestational Age by Ultrasound. Glob Libr Women's Med. 2008. https://doi.org/10.3843/glowm.10206

23. Abramowicz J, Sheiner E. Ultrasound of the placenta: a systematic approach. Part I: imaging. Placenta. 2008;29(3):225-40. https://doi.org/10.1016/j.placenta.2007.12.006

24. Granfors M, Stephansson O, Endler M, Jonsson M, Sandström A, Wikström AK. Placental location and pregnancy outcomes in nulliparous women: A population-based cohort study. Acta Obstetricia et Gynecologica Scandinavica. 2019;98(8):988-96. https://doi.org/10.1111/aogs.13578

Received December 15, 2023, accepted July 17 2024, date of publication July 25 2024.

Deep Learning and Photoacoustic Technology for Microcirculation Classification: Comparison Between Smoking and Nonsmoking Groups

Hui Ling Chua and Audrey Huong

Department of Electronic Engineering, Universiti Tun Hussein Onn Malaysia, Parit Raja, Johor

ABSTRACT

Abstract: Smoking has a significant impact on microcirculation, but existing tools for monitoring circulation perfusion in the smoking group have different shortcomings. This preliminary study explores the feasibility of using an in-house assembled multispectral photoacoustic (PA) system to investigate and compare the microcirculation performance between smoking and nonsmoking subjects. For this purpose, pretrained Alexnet, Long Short-Term Memory (LSTM), and a hybrid Alexnet-LSTM network were employed for the prediction task. This research included five smoking and thirty-two nonsmoking participants in the investigations that involved two experimental conditions, i.e., at rest and arterial blood flow occlusion. The findings showed that the PA signals produced in the smoking group have generally smaller magnitudes and negligible differences (when comparing between the two experiment conditions) than their nonsmoking counterpart. The employed models performed superiorly with the highest accuracy of 90 % given by the hybrid model, followed by 80 % recorded for Alexnet and LSTM using nonsmoking data. The performance of these models is reduced when they are trained and tested using smoking data. Our study highlights the task complexity and difficulty in determining tissue microcirculation status in heavy smoking individuals, which has been attributed to their possibly pre-existing atherosclerotic conditions and the high carboxyhemoglobin (COHb) level. A longitudinal study of smoking habit-dependent microcirculation abnormalities in smokers could offer further avenues for investigation. Future research includes incorporating systematic experimental protocols and access to the participant's medical records to improve the performance of the clinical decision-making system used for field applications.

Keywords – *Microcirculation perfusion; photoacoustic; smoking; Alexnet; LSTM*

INTRODUCTION

Smoking increases the risks of various conditions, including lung cancer, heart disease, respiratory problems, and other significant health issues. It induces vasoconstriction, narrowing the blood vessels in microcirculation and reducing blood flow to organs and tissues. Consequently, oxygen delivery to the tissues is diminished, impairing their proper function. Smoking also increases blood viscosity, hindering nutrient and oxygen delivery through narrow microvessels; it promotes the formation of blood clots, obstructs microcirculatory vessels, and damages tissue. Tobacco smoke contains carbon monoxide (CO) as one of its toxic components. When tobacco is burned and inhaled, CO is absorbed into the bloodstream, significantly affecting microcirculation. CO causes adverse effects in humans by combining with hemoglobin to form carboxyhemoglobin (COHb), preventing blood from carrying oxygen.[1-2] Based on the reports of Silva,[3] there exists a close association between tobacco use and microvascular dysfunction, which is manifested by impeded blood flow.

Conventional technologies available to investigate microcirculation in the smoking population include Magnetic Resonance Imaging (MRI),[4] Pulse CO-oximetry,[5] and spectroscopy.[6–7] However, the use of MRI is limited because of its high operational cost and rigid working conditions. Investigation of microcirculatory performances based on tissue gas saturation using CO-oximeter and spectroscopy is limited by the light penetration depth and variable degree of light scattering from tissue heterogeneity.[8] Photoacoustic (PA) imaging, which combines the features of optical spectroscopy and deep penetration of acoustic technologies, has gained increasing interest as an alternative method in microcirculation flow abnormalities detection. The light illuminating a sample absorbed by chromophores in the skin produces thermal expansion, which generates acoustic waves that a transducer can detect. The peaks of PA signals are linearly associated with the sample properties, while the temporal characteristic of PA signals would disclose the physiological properties of the tissues. Traditionally, physicians, particularly radiologists, would review and examine medical images before deciding on treatment planning. These tasks are crucial in diagnostic radiography, involving challenging analysis and diagnosis based on visual images. Artificial Intelligence (AI) has become essential in assisting and enhancing these decision-making processes by providing accurate, reliable, and efficient interpretation of results. This technology has been actively studied for different PA applications; some recent AI efforts include Sumit et al. [9], who demonstrated using deep learning (U-Net model) for multi-target detection with simulated PA imaging datasets. Warrier et al.[10]combined optimization and deep learning approaches for detecting and classifying cancer tissues using multispectral PA imaging. The study by Mohajerani et al.[11] proposed a novel machine learning-empowered optoacoustic sensor for recognizing diabetes with different complications based on the signals recorded from phantom and skin surfaces (in the human experiments). The adopted machine learning approach used bagged ensemble trees to find the correlation and best fit between the data and its labels. Similar works were carried out by Liakat et al.[12] and Sei et al.[13]; the former developed an in-vivo noninvasive glucose sensor to predict glucose concentration using the least square regression technique and based on the photoacoustic measurement in the skin, whereas the latter study used regression technique to determine blood saturation using PA signals of blood samples.

To the authors' best knowledge, no works have been carried out to use deep learning and PA techniques to compare the microcirculation changes or flow abnormalities between smoking and nonsmoking subjects. This work aims to investigate and compare the performance of different deep learning models for microcirculatory status (i.e., during at-rest and perfusion occlusion in smoking and nonsmoking groups) classification using the PA method. All the computations were performed on a DELL laptop with 64-bit Windows 10, Intel® Xeon™ i7-1700M CPU @3.20 GHz. All simulations were done in MATLAB (2022b).

METHODS

Ethical statements: This study was approved by the local research ethics committee at Universiti Tun Hussein Onn Malaysia (RMC.100-9/139,4).

2.1 Photoacoustic (PA) detection system

The schematic diagram of the experimental setup is shown in Figure 1 (top). The illumination system consisted of two 5 mm ultra-bright transparent white light emitting diodes (model: 5LED-UL-W) filtered by color filters (model: FKB-VIS-10, Thorlabs) to generate five primary colors with a center light wavelength of 450 nm, 500 nm, 550 nm, 600 nm, and 650 nm. These wavelengths were selected as they encompass the absorption spectra of hemoglobin (i.e., oxyhemoglobin and deoxyhemoglobin) required for analysis. The light modulation for illumination of the target area was achieved using an Acousto Optic Modulator (AOM) controlled by a radiofrequency (RF) driver with a carrier frequency of 15 MHz. The AOM produced modulating signals required to illuminate the subject. The acoustic energy generated in the medium was detected using an ultrasonic flaw detector (EPOCH 650, Olympus Corp, Japan). A wideband bandpass filter with fixed cut-off frequencies (0.5–4 MHz) built into the flaw detector was used to filter out high-frequency noise. Figure 1 (bottom) shows the actual setup in the laboratory. During measurements, a transducer head was placed in contact with the skin, and acoustic gel was the coupling medium. The signals were recorded using the EPOCH 650 flaw detector for offline analysis.

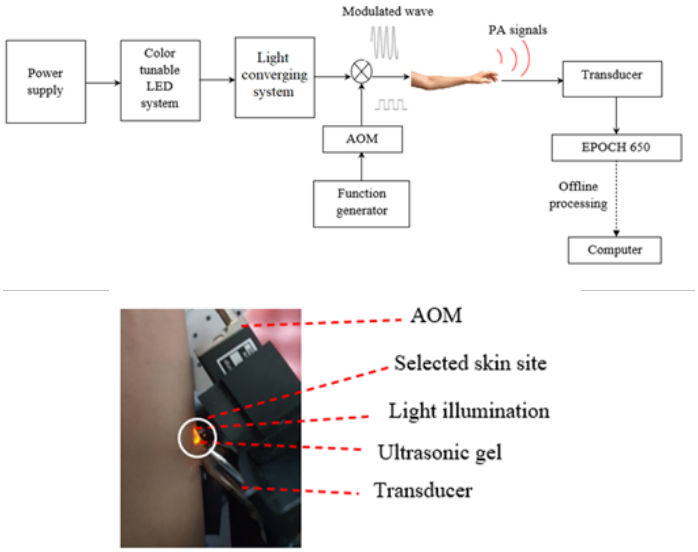

FIGURE 1. Schematic diagram of the PA system experiment setup (top) and a photograph of a color-tunable LED illuminating a subject's forearm during the measurement (bottom).

2.2 Subjects and protocol

Thirty-seven healthy individuals (19 males and 18 females, aged 21-30 years) were invited to participate in this research study. Among them, 32 were nonsmoking, and five were smoking participants, whose number of cigarette smoking years ranged from two to five years. The number of cigarettes smoked was between five to fifteen cigarettes a week. The local research ethics committee at Universiti Tun Hussein Onn Malaysia approved the study protocol (RMC.100-9/139,4). Before the study, these participants reported no known illnesses and were provided information about the experimental procedures, objectives, and potential risks. Upon enrolment, they provided their informed consent by signing a printed form. The experiment was conducted under two conditions: at rest and brachial artery blood flow occlusion to represent varying microcirculatory states.

The study commenced with the at rest experiment, where each participant was instructed to position the selected site beneath the illuminated light beam, starting with the light wavelength of 450 nm. The distance was maintained at 1 cm, and the angle of incidence was set at 45° from the source, as depicted in Figure 1 (bottom). Five signals were recorded from the same target site before varying the incident light wavelength. During the systolic occlusion experiment, a blood pressure cuff (model no. CK-110) was applied to the participants' upper left arm, i.e., by exerting a pressure of 140 mmHg for 30 seconds to induce ischemia, before the same data collection protocol was repeated. Inflating the cuff around the arm temporarily blocked blood flow, inducing an ischemic state in tissues below the cuff. This process promotes changes in the functional microcirculation by reducing the supply of oxygen-carrying blood to the lower extremities. This produces pathological conditions similar in patients with peripheral artery and vascular diseases. These procedures were applied to both smoking and nonsmoking (as the control group) individuals. The recorded screenshot signals were saved onto a microSD memory card using the flaw detector's built-in function for subsequent offline processing and analysis.

2.3 Signal pre-processing and dataset handling

Even though the produced PA signals are in 1D time series, the EPOCH 650 device has no function to save the raw signals. Therefore, a signal restoration approach was employed to convert the screenshot of the image saved on a microSD card into a vector representation or matrix format suitable for use with a time-based deep neural network (i.e., LSTM). This was facilitated by leveraging the distinct color contrast in the image, wherein the measured signal is depicted in green against a dark background. The image was first converted into a binary image using the im2bw function before the 1D matrix was obtained from the rows and columns of the image. The PA signal, X, from each measurement is of size 1 × 494 (i.e., X_1 ..., X_{494}), which was fed into the network input layer for further classification and analysis.

The original PA signals did not provide a satisfactory result in the pre-experiment investigations using the LSTM network. Therefore, time-dependent moments were used. The moments' extraction is by using the tfsmoment function, and this study considered signal variance (order, n=2), skewness (n=3), and kurtosis (n=4) as the input features in the prediction of microcirculation status. The smoking PA images and the corresponding moments were randomly divided into a 40/20/40 % split for training, validation, and testing sets, rendering 20/10/20 images for convolutional-based models and 60/30/60 signals for the LSTM network. The nonsmoking dataset divided using the split ratio of 46/28/26 % giving 160/100/90 images and 480/300/270 signals used for convolutional-based models and LSTM, respectively.

2.4 Deep learning networks and model training

This study recruited pre-trained Alexnet, LSTM, and a hybrid model for microcirculation flow abnormalities classification based on the measured PA signal. AlexNet and the hybrid model take color (RGB) images as the input, while the moments calculated from 1D PA signal in section 2.3 is used as the input of LSTM. Modification and the use of these models are described in sections 2.4.1 and 2.4.2; these models were optimized for the problem by searching for the best hyperparameter settings in section 2.4.3.

2.4.1 Convolutional-based models

The convolutional-based models used in this work comprised the pretrained Alexnet and hybrid CNN-LSTM model shown in Figures 2 and 3. The input of these models was changed to 494 × 329 × 3, consistent with the original PA image size recorded from the system.

In Alexnet, the network's last fully connected (FC) was modified to two neurons representing: "0" for the normal class and "1" for the pathological (or abnormal) class. A dropout layer of 0.50 was placed between each FC layer in Figure 2 to reduce network overfitting. Meanwhile, the Alexnet-LSTM shown in Figure 3 was proposed to extract spatial and temporal features from the screenshot PA images. A batch normalization layer is added to this hybrid model to normalize inputs for the subsequent layer. The upper layers of this architecture (i.e., Alexnet) are to extract spatial information from the input image. The extracted abstract information is passed through a flattened layer, converting the feature map into one-dimensional data. This sequential data is fed into the LSTM network to extract the temporal patterns. This time-recurrent network consists of 500 hidden layers, which was decided during pre-experiment tests. These layers are connected to FC layers and dropout layers of 0.2 to improve model generalization. The output of the FCs is fed to a Softmax to calculate class probabilities.

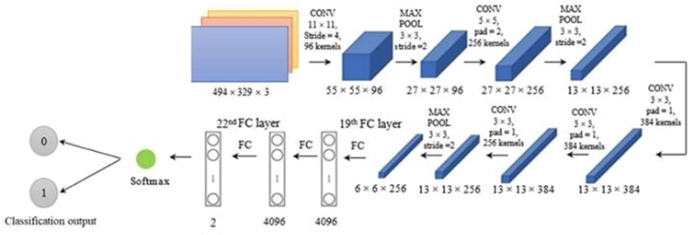

FIGURE 2. Architecture of Alexnet model.

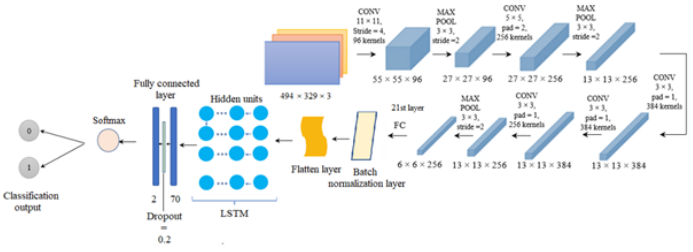

FIGURE 3. Architecture of the proposed hybrid Alexnet-LSTM model.

2.4.2 Time-based deep neural network

The temporal recursive network, LSTM, was also chosen for the task due to its adeptness in handling sequential data and addressing short-term memory challenges. Its architecture consists of an input layer, taking the calculated moment features described in section 2.2 as the input signals, followed by a sequence of 155 hidden layers to extract their essential temporal features. These are followed by six FC layers, whose sizes progressively decrease from 40 to 30, 20, 10, 5, 3, and 2. While no definitive method for determining FC sizes exists, this study adopted a diminishing sequence to simplify the model's structure, as shown in Figure 4. A dropout layer with a value of 0.1 is incorporated after each FC layer to prevent the risk of overfitting, except for the final layer. The output from the final FC layers is fed into a Softmax classifier to classify a signal into two categories (i.e., 0: normal and 1: pathological condition).

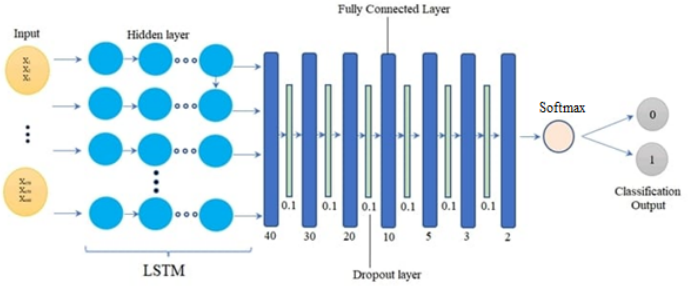

FIGURE 4. Architecture of the LSTM model.

2.4.3 Hyperparameters selection and model training

The classification models in Figures 2–4 were trained using the ADAM optimizer, known for its fast computation and quick convergence, while other important hyperparameters in Table 1 were adjusted manually.

TABLE 1. The Tuning Range of the Considered Hyperparameters and the Chosen Values

Parameter	Models	Limit		Step of change	Optimum hyperparameter
		Lower	Upper		
Epoch number	Alexnet	1	100	10	50
	LSTM	1	4000	100	500
	Hybrid	1	100	10	50
Mini Batch size	Alexnet	2	128	2^n, where n = 2,3…7	16
	LSTM	2	2048	2^n, where n = 2,3…11	32
	Hybrid	2	128	2^n, where n = 2,3…7	16
Initial learning rate	Alexnet LSTM Hybrid	5 × 10-4	1	5 × 10-4	5 × 10-4
Gradient descent threshold	Alexnet LSTM Hybrid	1×10^{-3}	1	$1e^{-n}$, n = 3, 2, 1, 0	1×10^{-3}

The optimal hyperparameters setting differed depending on the datasets and models used. Two-hundred sets of combinations consisting of different values in Table 1 were attempted in search for the best hyperparameters. The prediction accuracy fluctuated between 19% and 100%, while the training times varied from 56 to 154 minutes. This study identified the best combination based on the set that produced the highest training accuracy, such as 100 % for data of all wavelengths. The same optimum hyperparameters setting {epoch no., minibatch size, learning rate and gradient threshold} has been found for Alexnet and hybrid model as {50, 16, 0.0005, and 0.001} and {70, 16, 0.0001, and 0.001}, respectively, for smoking and nonsmoking data, and {500, 32, 0.0005, and 0.001} and {3000, 256, 0.0001, and 0.001}, respectively, for LSTM.

2.5 Score fusion strategy

This study used a combined prediction score to enhance the system's classification confidence. The class probability from models trained with each wavelength (i.e., 450 to 650 nm) was combined through summing to give the final score. This strategy is coined as the fusion method. An example of the fusion technique is shown in Figure 5.

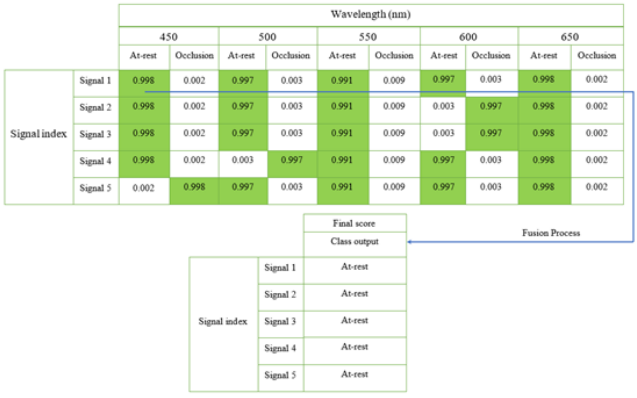

FIGURE 5. Fusion technique for final classification of microcirculatory status.

2.6 Performance metric

The effectiveness of the trained models used in this study is evaluated using classification accuracy shown

in Equation (1). This performance metric measures the degree of closeness of predictions to actual values.

$$\text{Accuracy} = \frac{\sum_{i=1}^{T} \frac{TP_i + TN_i}{TP_i + TN_i + FP_i + FN_i}}{N} \quad (1)$$

T denotes the total number of data and N denotes the total number of class labels ($N = 2$). A true positive (TPi) is when the abnormality for signal i is correctly detected. A false positive (FP) is the percentage of normal data misclassified as abnormal, a false negative (FN) is an abnormal signal class member incorrectly classified as normal, and a true negative (TN) is the correct prediction of normal PA signal.

RESULTS

Smoking individuals are known for having a high risk for vascular diseases; thus, the blood occlusion procedure is applied to these individuals to allow investigation of system sensitivity in this group of populations. Figure 6 compares the peak of PA signals at different wavelengths for smokers and nonsmokers under at-rest and occlusion conditions. It can be observed that the PA signals from nonsmoking subjects have overall higher amplitude values under both at-rest and occlusion conditions as compared to smoking subjects.

The PA produced from both (smoking and nonsmoking) groups exhibit the same pattern. The signals produced under at-rest and occlusion conditions peak at 450 nm and 550 nm, respectively, and the differences (between the different experimental conditions) are considerably negligible for wavelengths 500 nm, 600 nm, and 650 nm, as shown in the figure.

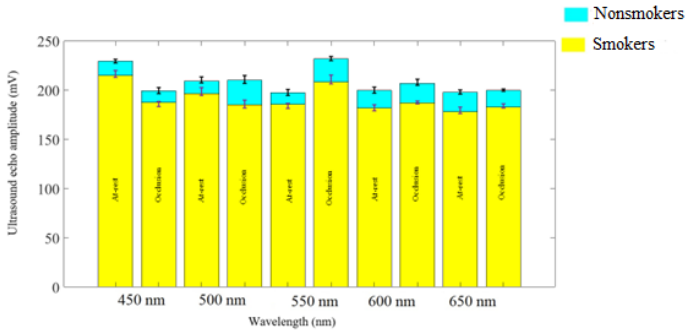

FIGURE 6. Mean and standard deviation (represented by error bar) of PA echo amplitudes produced in smokers and nonsmokers under different illumination wavelengths.

The classification results following the fine-tuning of the employed models using the nonsmoking and smoking data and from score fusion technique are shown in Figures 7 and 8, respectively. The training and testing of the Alexnet and hybrid model used screenshot images, while signal moments described in section 2.3 are used as the input to the LSTM.

DISCUSSION

PA technologies, such as skin glucose and oxygen saturation detections, have been extensively tested in various diagnostic imaging applications. However, the use of this technology in the detection of compromised microcirculation, especially in the smoking population, has not been investigated. This research compares changes in blood perfusion under induced pressure in individuals with

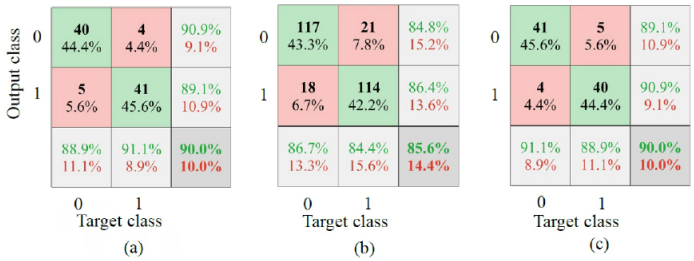

FIGURE 7. Confusion matrix of (a) Alexnet, (b) LSTM, and (c) hybrid model in classifying microcirculation status in nonsmoking subjects based on PA images and signals (class 0: normal, 1: abnormal).

FIGURE 8. Confusion matrix of (a) Alexnet, (b) LSTM, and (c) hybrid model for classification of microcirculation status (class 0: normal, 1: abnormal) in smokers based on PA images and signals.

different smoking habits based on PA signals produced under visible wavelengths illumination.

The fundamental principle of the adopted PA technology is that the magnitude of the PA signal produced by

tissue depends on the hemoglobin variants' absorption properties, wherein the oxyhemoglobin light absorption peaks at 450 nm[14] while deoxyhemoglobin absorption peaks at 550–560 nm.[15] The absorption properties of these hemoglobin variants are similar for the remainder employed wavelengths (i.e., 500, 600, 650 nm). This trend was observed in Figure 6. This diagram revealed the highest PA signal magnitude recorded at 450 nm illumination, while 550 nm produced, generally, the highest ultrasonic echo amplitude under blood flow occlusion condition, where the regional tissue deoxygenated blood is rich due to impeded oxygen-carrying blood from flowing into the lower arm (measurement site). The PA signals obtained from smokers have considerably weaker echoes than nonsmokers, with a mean relative percent difference of 9.5% across all wavelengths and experiment conditions. This relative percent difference between nonsmoking and smoking results is divided by the two results. There is also high consistency in PA signals obtained from smoking subjects for both experiments. The COHb level is generally high in smokers, and the absorption spectrum of this hemoglobin variant, associated with the risk of inadequate oxygen delivery,[16] is considerably less prominent as it overlaps with that of oxyhemoglobin and deoxyhemoglobin in the visible wavelength range. While the dominance of light absorption of COHb could be the primary cause of the observations on the lower magnitude in the produced signals, we do not rule out the possibility of the already impaired microcirculation function or pre-existing atherosclerotic conditions in this group of participants, causing negligible differences in the readings between the at rest and external exerting pressure experiment.

Figure 7 shows the models' classification performance tested on nonsmoking (healthy) participants. The networks trained and tested on healthy subjects' data revealed considerably good accuracies ranging between 85.6 and 90%, suggesting the consistent performance between the convolutional-based models and temporal-based LSTM, and their feasibility in classifying normal and abnormal (occluded) microcirculation performance in nonsmoking individuals. Meanwhile, the results in Figure 8 reveal that the performance of these models decreased in the compromised microcirculation status (i.e., occlusion condition) detection. Even though the hybrid model achieved consistent classification accuracy (i.e., 90%), followed by Alexnet and LSTM with a classification accuracy of 80%, this group's FN rate is high (~20-40%). An investigation was carried out on the misclassified data, and it was found that they belong to the same subject, who reportedly smokes about fifteen cigarettes a week. All signals from this subject, the heaviest smoker among the five recruits, were misclassified as normal. One possible reason is that the atherosclerotic conditions, one of the known complications in smokers, could have been detected during at-rest condition, so further exerting external pressure on the limb during the blood occlusion experiment produced near negligible changes, as observed in the smoking group in Figure 6.

For the above-stated reasons, this work does not rule out the possibility of the models is overfitting to the normal (i.e., at rest) class in the smoking group, largely due to the negligible differences in the PA signals between at rest and occlusion conditions, compromising the classification performance of the models. Although an insufficient dataset (i.e., in the smoking group) could lead to biased predictions, the good performance of the models using nonsmoking data in Figure 7 and the high misclassification rates of pathological condition (i.e., between 20-40 %) that agreed well with the observations of,[17] and[18] indicating a certain degree of reliability of our findings.

It must also be mentioned that this study has no access to the participants' information, such as previous health records, and has not included their diet and environmental factors in the experimental design; these factors may influence the results and analyses of the study. Therefore, the future of this study includes recruiting more participants with various backgrounds and smoking habits and adopting a systematic experimental procedure (e.g., convenient access to patient's medical records) to investigate the blood microcirculatory performance between healthy and unhealthy (or patient) groups to enhance the validity of the research findings. The improved clinical decision-making system can be integrated into the proposed PA system and considered an alternative imaging tool to facilitate the investigation of tumor angiogenesis and microvascular dysfunction, allowing early identification of compromised microcirculation and preventing further complications.

CONCLUSION

This paper demonstrated the use of deep learning-incorporated PA technology to investigate blood perfusion in nonsmoking and smoking subjects. The results showed that the proposed hybrid Alexnet-LSTM model performed better than the conventional Alexnet and LSTM models in the classification of microcirculation changes in both smoking and nonsmoking groups. These models performed inferiorly with high misclassification rates of 20–40% in the detection of compromised perfusion in the smoking group. This observation is attributed to the compromised perfusion in this group of subjects. This explains the negligible change observed after exerting external pressure impeding the (oxygen-carrying) blood flow and the limited smoking dataset for training the models. Future works include recruiting volunteers of diverse backgrounds, profiles, and smoking status to enhance the validity and practical application of existing findings in the healthcare system.

CONFLICTS OF INTEREST

No potential conflict of interest relevant to this article was reported.

FUNDING

Ministry of Higher Education (MOHE) Malaysia through Fundamental Research Grant Scheme (FRGS/1/2020/TK0/UTHM/02/28)

REFERENCES

1. Prockop, LD and Chichkova, RI. Carbon monoxide intoxication: an updated review. J Neurol Sci 2007;262:122–130. doi: 10.1016/j.jns.2007.06.037.
2. Fagerstrom, KO. Effects of a nicotine-enriched cigarette on nicotine titration, daily cigarette consumption, and levels of carbon monoxide, cotinine, and nicotine. Psychopharmacol (Berl) 1982;77:164–167. doi: 10.1007/BF00431941.
3. Silva H. Tobacco use and periodontal disease—the role of microvascular dysfunction. Microcirc Health Disease 2021;10(5): 441. doi: 10.3390/biology10050441
4. Chen NC, Chang WN, Lui CC, et al. Detection of gray matter damage using brain MRI and SPECT in carbon monoxide intoxication: a comparison study with neuropsychological correlation. Clin Nuclear Med 2013;38:e53-e59. doi: 10.1097/RLU.0b013e31827082a7.
5. Ozcan N, Ozcam G, Kosar P, et al. Correlation of computed tomography, magnetic resonance imaging and clinical outcome in acute carbon monoxide poisoning. Rev Bras Anestesiol 2016;66:529–532. doi: 10.1016/j.bjane.2014.05.006.
6. Parks J and Worth HG. Carboxyhemoglobin determination by second-derivative spectroscopy. Clin Chem 1985;31:279–281.
7. Huong AKC, Mahmud WMH, Tay KG, et al. Smoking status classification by optical spectroscopy and partial least square regression, J Physics: Conference Series 2019;1372:012031. doi: 10.1088/1742-6596/1372/1/012031.
8. Culnan DM, B. Craft-Cffman B, Bitz GH, et al. Carbon monoxide and cyanide poisoning in the burned pregnant patient: an indication for hyperbaric oxygen therapy. Ann Plast Surg 2018;80(S106).doi:10.1097/SAP.0000000000001351.
9. Sumit A, Suresh T, Garikipat A, et al. Modeling combined ultrasound and photoacoustic imaging: Simulations aiding device development and artificial intelligence. Photoacoustics 2021;24. doi:10.1016/j.pacs.2021.100304.
10. Warrier GS, Amirthalakshmi TM, Nimala K, et al. Automated recognition of cancer tissues through deep learning framework from the photoacoustic specimen. Contrast Media Molecular Imag 2022. doi: 10.1155/2022/4356744
11. Mohajerani P, Aguirre J, Omar M, et al. Machine-learning powered optoacoustic sensor for diabetes progression. Medrxiv. 2021. doi:10.1101/2021.03.17.21253779
12. Liakat S, Bors KA, Xu L, et al. Noninvasive in vivo glucose sensing on human subjects using mid-infrared light. Biomed Opt Express. 2014;5:2397–2404. doi: 10.1364/BOE.5.002397.
13. Sei K, Fujita M, Hirasawa T, et al. Measurement of blood-oxygen saturation using a photoacoustic technique in the rabbit hypoxemia model. J Clin Monitor Comput. 2018;33:269–279. doi: 0.1007/s10877-018-0166-8.

14. Nguyen DD, Pang JY, Madill C, et al. Effects of 445-nm laser on vessels of chick chorioallantoic membrane with implications to microlaryngeal laser surgery. Laryngoscope 2021;131. doi: 10.1002/lary.29354.

15. Friedmann D and Verma KK. Enhanced perception of deoxygenated hemoglobin for the visualization of lower-extremity reticular veins. Dermatol Surg 2024;50(2):207–209. doi: 10.1097/DSS.0000000000003974.

16. Azizah RN, Puspitasari A and Lestari I. Relationship of carboxyhemoglobin (CoHb) and hemoglobin (Hb) levels in active smokers in gresik regency. Internat J Adv Health Sci Technol 2024;4(1):8–11. doi: 10.35882/ijahst.v4i1.291.

17. Low BH, Lin YD, Huang BW, et al. Impaired microvascular response to muscle stretching in chronic smokers with type 2 diabetes. Frontier Bioengineerin Biotechnol: Section Biomechanics 2020;8. doi: 10.3389/fbioe.2020.00602.

18. Hashimoto H. Impaired Microvascular vasodilator reserve in chronic cigarette smokers: a study of post-occlusive reactive hyperemia in the human finger. Japan Circulat J 1994;58:29–33.